American Journal of Engineering Research (AJER)
e-ISSN: 2320-0847 p-ISSN : 2320-0936
Volume-13, Issue-3, pp-72-93
www.ajer.org
Research Paper Open Access

Evaluation of the Rosetta Promontory Stability and Shoreline Changes and Proposed Solutions, Northwest Coast, Egypt

Khyal A. Zahra
Associate Professor Researcher and Head of Coastal Engineering Department, Coastal Research Institute, National Water Research Center, P.C. 21514, Alexandria, Egypt, E-mail: khyalahmed@hotmail.com

ABSTRACT
The Rosetta Promontory (RP) on the northwestern coast of the Nile Delta (ND) is exposed to serious issues with erosion and accretion owing to climate change and sea level rise. The main problems in Rosetta revetments (RR) are the lack of structural functions and the deterioration of the structure with fractures and damage of some Dolos units of protective shield layers. This leads to minimizing its interlocking, and hydraulic instability leading to failure in the future. The study examines the effect of broken units on revetment stability and efficiency through the FLOW 3D numerical model to assess the interaction between the fluid and the revetment with the existence of broken units. The study revealed the velocity of induced waves increased with the increase of the ratio between the wave height and water depth. Consequently, moving broken units has a significant effect on other units' stability. Moreover, the erosion processes migrated to both RP sides; east of the eastern and west of the western revetments. From 1985–2022, the annual erosion rate on the eastern RR was 38 m/year. The study recommended removing the broken parts from the revetment to save the other stable units, in addition, constructing two jetties at the Rosetta branch mouth to protect from sedimentation and enhance navigation, and building a submerged breakwater in front of the RR to absorb wave energy, as well as deepening the foundation level of the RR toe to (-8.0 m) below mean sea level and expanding it by 10 meters.
KEYWORDS:
Fluid-structure interaction, FLOW 3D, erosion, Rosetta Promontory, stability, shoreline change.

Date of Submission: 13-03-2024 Date of acceptance: 27-03-2024

I. INTRODUCTION

Preamble

Owing to the location of the Nile Delta at the center of Egypt's population, extensive industrial and agricultural infrastructure, and extensive fisheries, it is important socioeconomically to Egypt. Due to various coastal processes like erosion, accretion, and land subsidence, the shoreline has been altering constantly. Egypt's water flow was managed by constructing many dams and barrages on the Nile River. According to Ghoneim et al. (2015), these include the Delta Barrage (1861), the Assuit Barrage (1902), the Edfina Barrage (1950), the Aswan Low Dam (1902), and the Aswan High Dam (AHD) (1964). The amount of sediment flux that the Nile River carries to the Mediterranean Sea has been quantitatively decreased by the AHD and other man-made constructions across the river. Shalash (1982) states that the AHD has a 98% trapping effect, meaning that only a small quantity of the material, mostly silt and clay, travels downstream and nearly all of the sediment stays in Lake Nasser upstream of the dam. As a result, many beaches are losing their sand, and these beaches are becoming devastated by waves and strong sea currents. Low-lying areas of the ND are flooding and being overtaken by seawater due to climate change and sea level rise. Numerous initiatives have been implemented to save the Nile Delta's shoreline. Rosetta Promontory is the area where these processes are most noticeable. Numerous studies have been suggested to address the changes affecting the Rosetta Promontory. These investigations included an analysis of the historical maps (Frihy et al., 1991). Others (Aly et al., 2012) have drawn shorelines using satellite imagery. Several studies (Deabes, 2017) computed the rates at which the shoreline is changing, while other studies (Elsayed and Mahmoud, 2007; El Banna, 2007) looked at the effect of hard structure on the shoreline orientation.

1.1 The Area Study

From Port Said (east) to Alexandria (west), the northern Nile Delta stretches for roughly 240 kilometers. Three promontories—two at Damietta and Rosetta and one intermediate relict at Burullus—interrupt the gently arcuate topography of the Delta coastline. An accreted saddle and embayment divide these three promontories (Frihy & Komar, 1993). Figure 1 shows the location of the Rosetta promontory, which is on the Mediterranean shore in the western part of the Nile Delta, east of Abou Quir Bay around 60 kilometers east of Alexandria City. According to El Sayed et al. (2007), water-carrying sediments from the ancient Canopic and Sebennytic Nile branches were diverted, forming the modern Rosetta Branch between 500 and 1000 AD. Rosetta Promontory continued to expand and deposit material until the early 1900s when it approached the sea at a distance of roughly 14 km (CoRI/UNESCO/UNDP, 1978). After the Low Aswan Dam was built in 1902, the regression process started, as Figure 2 illustrates (Fanos et al., 1995). Numerous methods were employed to calculate the pace of shoreline change along the Rosetta Promontory. Between 1900 and 1991, the western and eastern shorelines of Rosetta Promontory receded by 5.8 and 4.4 km, respectively. (Fanos et al., 1995). According to Ghoneim (2009), the Rosetta Promontory's ground area lost around 9.5 km2 between 1972 and 2003, while the shoreline retreated by 3 km during that time.

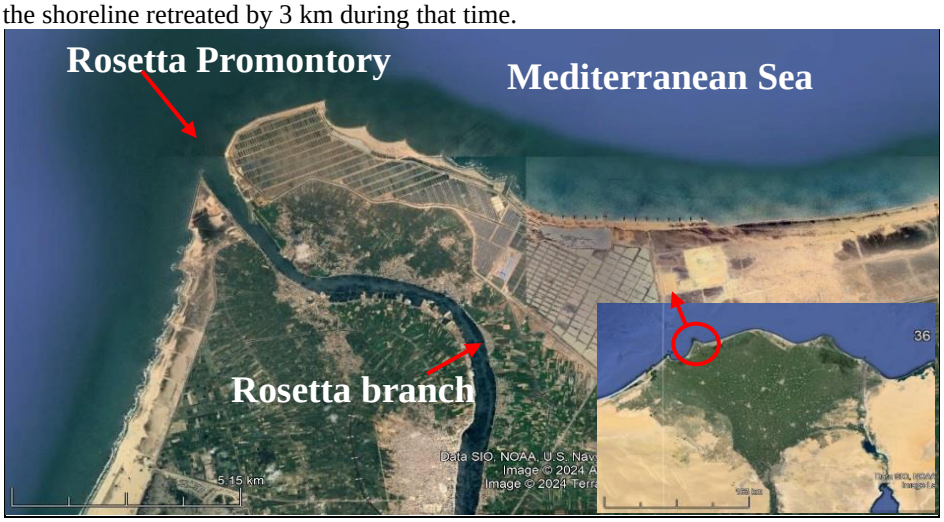

Figure 1: Rosetta Nile River Branch and Rosetta Promontory at the Mediterranean Sea.

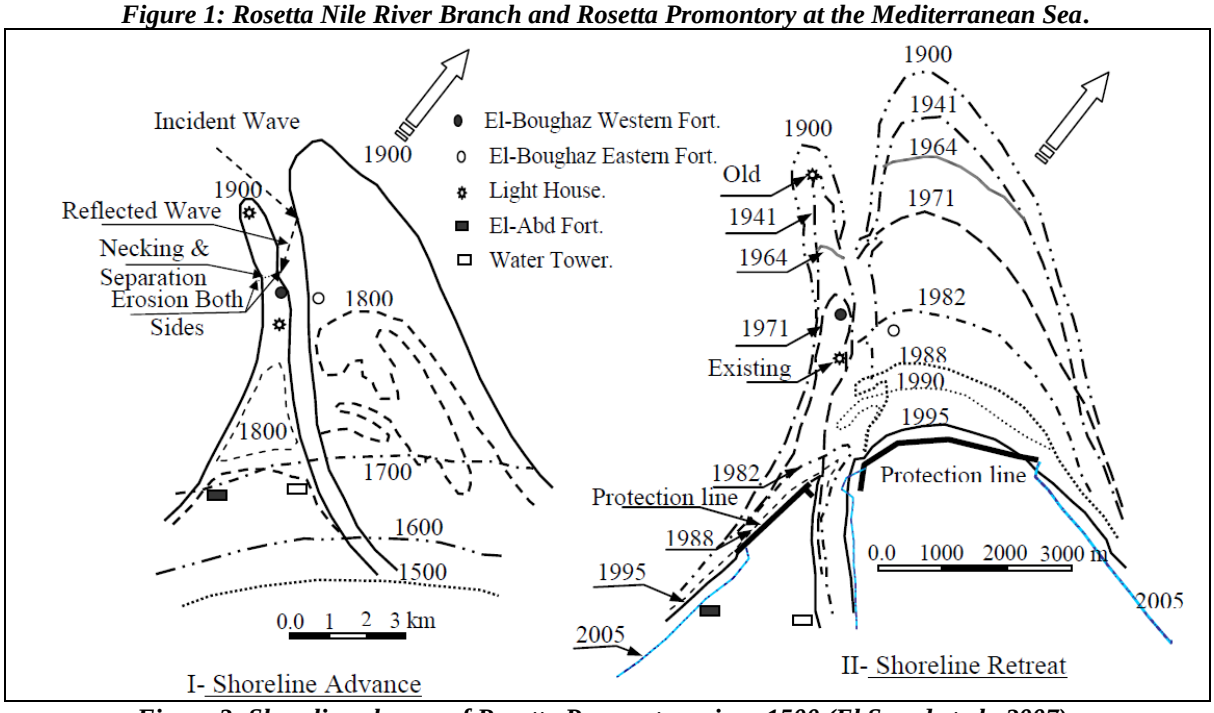

Figure 2: Shoreline change of Rosetta Promontory since 1500 (El Sayed et al., 2007).

According to calculations, the maximum erosion rate was 137 m/year (Ghoneim et al., 2015). As illustrated in Figure 3, protective engineering structures have been implemented to address Rosetta's issues with erosion and accretion, such as revetments and groins. Two inland revetments measuring 3.5 and 1.5 km were

constructed on the Rosetta Promontory sides, respectively, between 1986 and 1991 (Fanos, 1999). This revetment extends six meters above and below mean sea level (MSL) (Fanos, 1999). The sea wall is 48 to 70 meters wide, 6.75 meters high, and has an armor weight of 4 to 7 tons. Due to the movements of waves and currents as well as a lack of sediment delivery to the promontory, the ground was eroded before these revetments. Following the two revetments' completion, the land and shoreline were successfully prevented from retreating (El-Gamal, 2012); however, erosion occurred alongshore on the eastern and western sides, respectively. As a result, the eastern revetment side was extended for around 250 meters, according to Abd-Elmonem, Ibrahim M., et al. (2022). Around 40 short, submerged rubber-tube groins were constructed in 2000 along the western revetment at its southern edge to secure a two-kilometer gap. Building a basalt wall to protect neighboring sites such as Tabiyat El-Abd Fort was necessary after these collapsed and were demolished. To slow down the rate of erosion, 15 groins were implemented between 2003 and 2005 on both sides of the Rosetta revetment. Of these, five rubble mound groins with a length of 400 to 500 m and a spacing of 800 to 900 m (Frihy et al., 2008) were built to safeguard the eastern side.

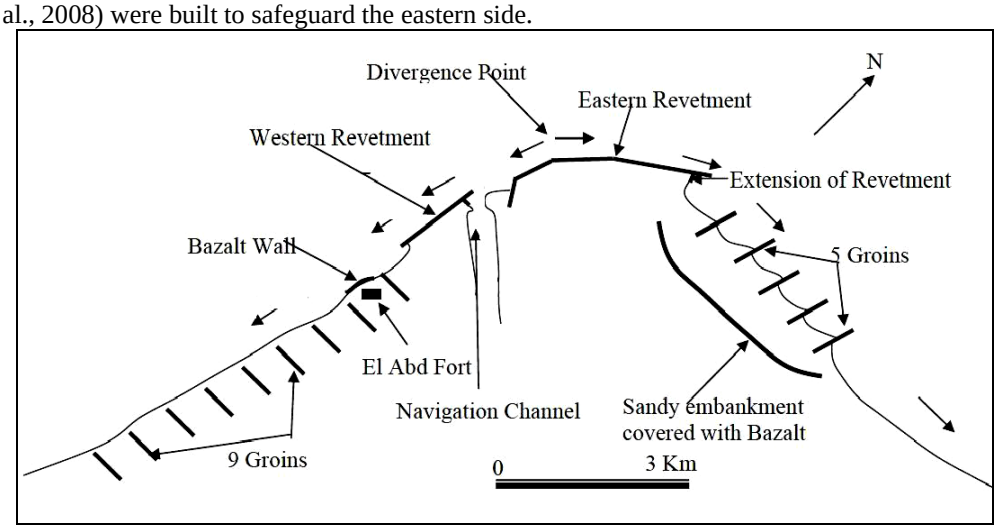

Figure 3: Rosetta Promontory protection measures (El Sayed et al., 2007)

Conversely, the Rosetta Nile branch experiences sedimentation issues. To provide a fishing boat navigation channel, two dredging projects are carried out for the Rosetta branch. Additionally shielded from wave effects is the branch bank of the Rosetta branch at its mouth. Despite all the protective measures taken, the Rosetta promontory continued to face erosion and sedimentation issues in addition to the structural and functional degradation of the revetment. Furthermore, the degradation of the Revetment sections and the fracture of several Dolos units were brought on by the strong waves and currents near the Rosetta branch mouth. Therefore, in 2019, the Shore Protection Authority repaired the western revetment at its eastern head. There are two stages to the project:

- The first step spanned roughly 350 m from the start of the western Revetment and involved replacing two rows of the shattered Dolos along the crest with the same weight (4.0 tons).
- The second phase involved building a new revetment in front of the previous one. The cross-section of the new revetment was composed of tetrapod 6-ton units for the armor layer, 2-3-ton dolomite stones for the toe layer, 0.5-1-ton for the underlayer stones, and 10-200 kg of weight stones for the core.

The project is seen as expensive for the Egyptian economy because it costs roughly 64.429 million Egyptian pounds (Abd-Elmonem, Ibrahim M., et al., 2022).

1.3 Problem description

The main problem is the erosion in front of the revetment towards the sea and the decline of the sea bed level to the critical level, which is the surface of the wall toe, on its way to exposing the foundations. Then, it leads to failure due to instability. The second problem is the deterioration of the revetment Dolos units due to cracks resulting from the rust of the skewer bars and sometimes fractures in the unit flank. This reduces the unit weight and reduces the interlocking between units, which is an important factor in barrier stability. Furthermore, the lack of sediment flux carried by the Nile as a result of the construction of the AHD led to an erosion problem that decreased the land area near the coastal zone. It has affected the socio-economic state of the promontory through agricultural, industrial, and fishing facilities. Also, the accretion problem that leads to the siltation of the inlets and navigation channels leads to the shoaling of the exits and deterioration of the Rosetta area's fishing, navigation, and ecosystem.

1.4 The objectives

The objectives of this study are to assess the rates of shoreline change from 1985 to 2022, the impact of protective structures on these rates, evaluate the barrier status in terms of construction and stability, examine the effect of broken units on revetment stability and efficiency, and propose solutions to overcome these problems.

II. MATERIALS AND METHODS

2.1 Methodology

To achieve the study objectives, the following activities have been combined:

1. The compilation of prior research in this area, as well as field investigation, and field measurements of hydrographic marine surveys, shoreline position measurements, sea level variations, wave measurements, and coastal protection measures.
2. Simulation of the fluid structural interaction through the application of CFD numerical model (FLOW 3D) to simulate the revetment stability.
3. Simulation of the hydrodynamic forces of waves on the base of the eastern revetment through the application of the DHI Mike Zero package numerical model.
4. Proposing solutions.

The Computational Fluid Dynamics (CFD) numerical model (FLOW 3D) solves Naiver-Stokes equations within nodes of the computational mesh by using the volume of fluid technique (Flow Science, 2009).

The DHI Mike Zero is a software package developed by the Danish Hydraulic Institute (DHI) for the numerical modeling of coastal and marine environments. It is a comprehensive software package that includes a suite of modules for simulating hydrodynamics, sediment transport, water quality, and ecology.

2.2 Data collection

2.2.1 Sea level data

Sea level change information is essential for planning protective measures, establishing shorelines, and constructing ports (Zahra, 2018b). They are used to estimate the amount of water that floods coastal areas. On the North Dakota coast, the micro-tidal semi-diurnal tidal regime is typical. Forty centimeters is the usual tidal range (Frihy and Deabes, 2011). Tide and ebb statistics are important when studying coastal projects, especially when looking at the areas where the sea and estuaries or drain mouths intersect. Their description of how the sea surface level fluctuates over time provided the foundation for the daily variations in sea level that were recorded at Rosetta City between January 2015 and January 2016 (Zahra, 2018b).

2.2.2 Marine Wave Data

Marine wave-induced long-shore currents are important to consider while analyzing inshore operations. When there is no sediment supply to the coast, waves and currents continue to act, causing beach erosion (Frihy et al., 2003). In 2004, wave climate data was measured with the InterOcean S4DW directional wave-current meter equipment (S4DW), which was located in front of the Idku Region (CoRI, 2004). The S4DW is composed of a pressure sensor and an electromagnetic current meter (Zahra, 2018b).

2.2.3 Shore-line data

One aspect of the dynamic coastal zone that is changing quickly is the shoreline. For coastal zone management, its movement as a result of erosion and accretion is a crucial concern (White and El-Asmar, 1999). Sea-level rise assessment, numerical model calibration and verification, and coastal protection design are all aided by the shoreline data. Shoreline changes can be examined using field data measurements or satellite images to determine the maximum annual retreat and the shoreline change of the study region. Due to the AHD's construction on the Nile River, which decreased the annual supply of sediment from about more than 0.12 billion tons to nearly zero at this point, the ND coast faces serious erosion issues (Smith and Abdel Kader, 1988). According to Frihy and Deabes (2011), the primary issue with these buildings is that they cause severe beach erosion on downdrift sides that might extend beyond the project area. Using multispectral remote sensing techniques and Landsat images covering the research area from 1985 to 2015, Balbaa, et. Al., 2020 derived the shoreline position data. The images were taken from the "Earth Explorer" webpage maintained by the USGS. The images have previously undergone geometric correction using the UTM projection at zone 36 N and the WGS 84 datum. Software called Erdas Imagine 15 was utilized to progress the analysis. In addition, the shoreline data of the area study was measured by the Coastal Research Institute (CoRI) for the period from 2008–2015, 2016, 2017, 2020, 2022, and 2023. The Digital Shoreline Analysis software (DSAS) was utilized to estimate the rates of coastline change. According to Heimelstoss et al. (2018), this operates inside the ArcGIS. A shoreline vector data time series' rate-of-change statistics are calculated by DSAS. The shoreline's displacement between the two dates was conducted to estimate the erosion/accretion pattern, then estimate the displacement category in m/yr.

2.2.4 Rosetta Revetment Data

To protect the shoreline, numerous protective structures are constructed. By breaking and dispersing wave energy, these structures safeguard the coastal area. This energy can be dispersed by about 60 to 70% through absorption by the protective structure body and between 30 and 40% by reflection (Tulsi, Kishan, et al., 2016). According to Andersen (2006), the structural body typically consists of armor layers, natural stone filters, and core layers. According to Deltares (2017) and Shand (2017), the armor layer serves as the first line of defense against wave attacks. It absorbs wave energy to lessen overtopping, run-up, and reflection while safeguarding the filter material below from strongly acting waves. Marine constructions like breakwaters, groins, seawalls, and harbors are frequently built using concrete armor units (Ciria, Cur, and Cetmef, 2007). In the maritime environment, concrete armor units are susceptible to a range of physical and chemical deterioration processes that may result in a complete structural failure (Ibrion M, et al., 2020). Insufficient hydraulic or structural stability can lead to physical harm to concrete units (Oliver J. et al., 1998). By making these units more slender than simple cube units, armor units can increase their hydraulic stability (displacement resistance) and require less weight to reduce the number of moving units (Rock Manual, 2007). Conversely, increasing the units' slenderness may reduce their structural stability (i.e., resistance to individual unit fracture) (Muttray M, and Reedijk B, 2008). As a result, structural instability typically happens before hydraulic instability, making the cylinder units more prone to rupture more quickly than the massive units. Empirical formulas assessed in physical model tests can be used to approximate hydraulic stability (Pedro, J., 2009). However, there are other methods for studying structural stability, including numerical simulations (Guo L., et al., 2015), physical models (Mitsui, J., et al., 2010), and the placement of strain gauges in specific units for evaluation (Myrick, G. B., & Melby, J. A. 2005). Concrete exposed to the coastal environment deteriorates due to chemical interactions between the cementitious components and seawater. Numerous investigators examined the impact of Chemical Attacks on the harm caused by waves on concrete in maritime environments (Ting, M. Z. Y., et al., 2021). Damage to the armor layer typically destroys the marine structure, and there are numerous causes for this failure (Maddrell, R., 2006). The design weight of the units is established based on the fraction of the armor layer failure that is permitted to reach the economic weight (Viet ND, et al., 2008). The number of damaged units over a given area is commonly used to characterize damage; the accepted percentage of damaged units is between 1% and 5% of the total number of units on the breakwater's armor layer (Campos Á, et al., 2020). When the percentage of breakage units (fracture in their location) is greater than 15%, the armor layer collapses (USACE, 2011). It is necessary to take mitigation steps to improve the longevity of the structure, such as selecting the right concrete strength, utilizing the ideal slenderness, and implementing various repair techniques. There are numerous ways to evaluate the state of coastal construction (Hassanin A., and Jukes P, 2018).

2.2.5 Hydrographic Marine Survey Data

The CoRI started a program of surveying beach profiles in 1971. The profile lines run perpendicular to the coast and reach a maximum distance of 1200 meters from the fixed baseline, or roughly 6 meters below the surface of the water. The survey was conducted for the variation of sea bed level from 2008–2015, 2016, 2017, 2020, 2022, and 2023 in front of the Rosetta revetment at 15 marine profiles.

III. RESULTS, DATA ANALYSIS AND DISCUSSION

3.1 Sea level Variation

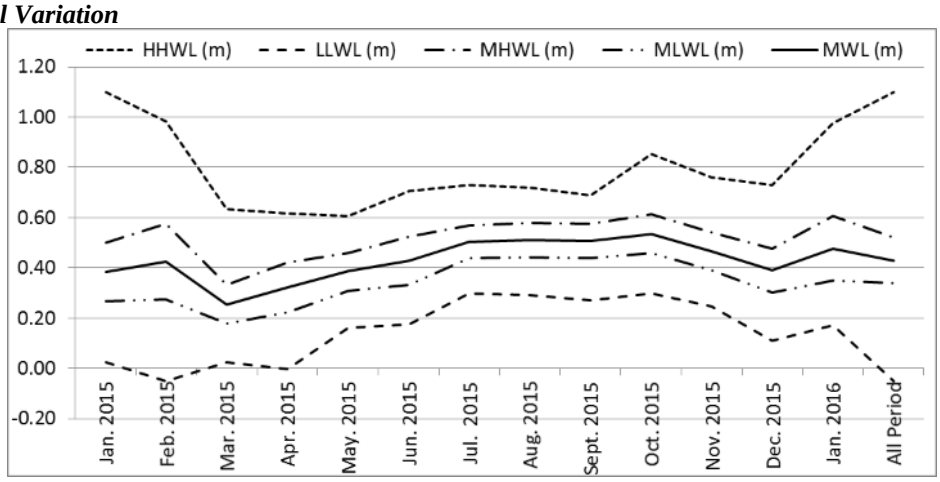

Figure 4: The daily sea level changes that were recorded at Rosetta City between January 2015 and January 2016 (CoRI, 2016, and Zahra, 2018b).

The sea level variations in Rosetta City between January 2015 and January 2016 as reported by CoRI (CoRI, 2016) are shown in Figure 4 (Zahra, 2018b). The information has been looked over and evaluated. The results of the analysis therefore showed that the sea level was around +0.40 m overall, with the lowest level occurring in February 2015, which is estimated to have been 0.05 m below zero sea level, and the highest level occurring in November 2015, at +0.76 m above MSL. Half-daily tides are generally experienced along Egypt's shore.

3.2 Marine waves

A study of the wave's data has confirmed the wave's features and direction. The analysis of these data thus shows that the maximum wave height in 2004 was over 4.5 meters, and the peak wave period was roughly 6.5 seconds (CoRI, 2004). Therefore, the dominant wave approach from the WNW and NW, as shown in Figure 5, is responsible for producing the eastward-flowing long-shore current and morphological alterations due to their extended length, especially during the winter (Zahra, 2018a).

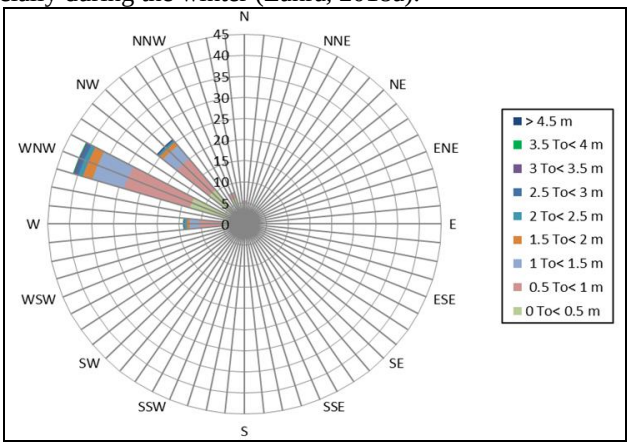

Figure 5: Rose waves of Idku Region, 2004 (Zahra, 2018a).

3.3 Shoreline

The shoreline's changes over time provide insight into its stability and response to accretion and erosion. The shoreline of the Rosetta Promontory is considered to be the most susceptible to erosion and sedimentation problems. The highest rate of erosion was concentrated at the tip of the promontory before the revetment's installation from 1988 to 1992, reaching around -39 m/y in the western sector and roughly -138 m/y in the eastern sector (Balbaa, et al., 2020). The erosion rate at the promontory's tip almost stopped (-1.9 m/y) when the revetment was built.

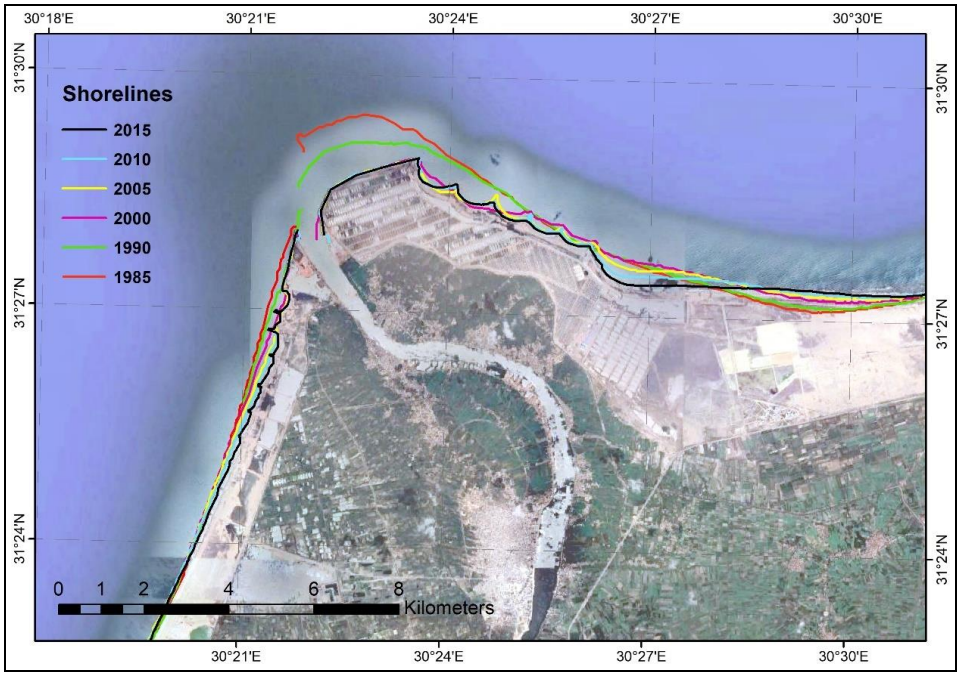

Figure 6. Rosetta Promontory shorelines (1985 to 2015) (Balbaa, et al., 2020).

The land was successfully prevented from retreating by the two revetments; however, erosion occurred alongshore on the eastern and western sides, respectively. Consequently, the eastern revetment was extended by approximately 250 meters, and five groins, each measuring approximately 500 meters, were built to safeguard the eastern side (Abd-Elmonem, et al., 2022), as shown in Figure 3. Figure 6 displays the shorelines of Rosetta Promontory and their shoreline position variations from 1985 to 2015 (Balbaa, et al., 2020), while Figure 7 illustrates the shoreline positions in November 2016, November 2022 from CoRI investigations, and in March 2024 through Google Earth. There is erosion in both the area east of the eastern revetment and west of the western revetment. The land retreat from 2016 to 2024 between the first two groins east of the eastern revetment is 33.75 m, while it is around 60 m west of the western revetment.

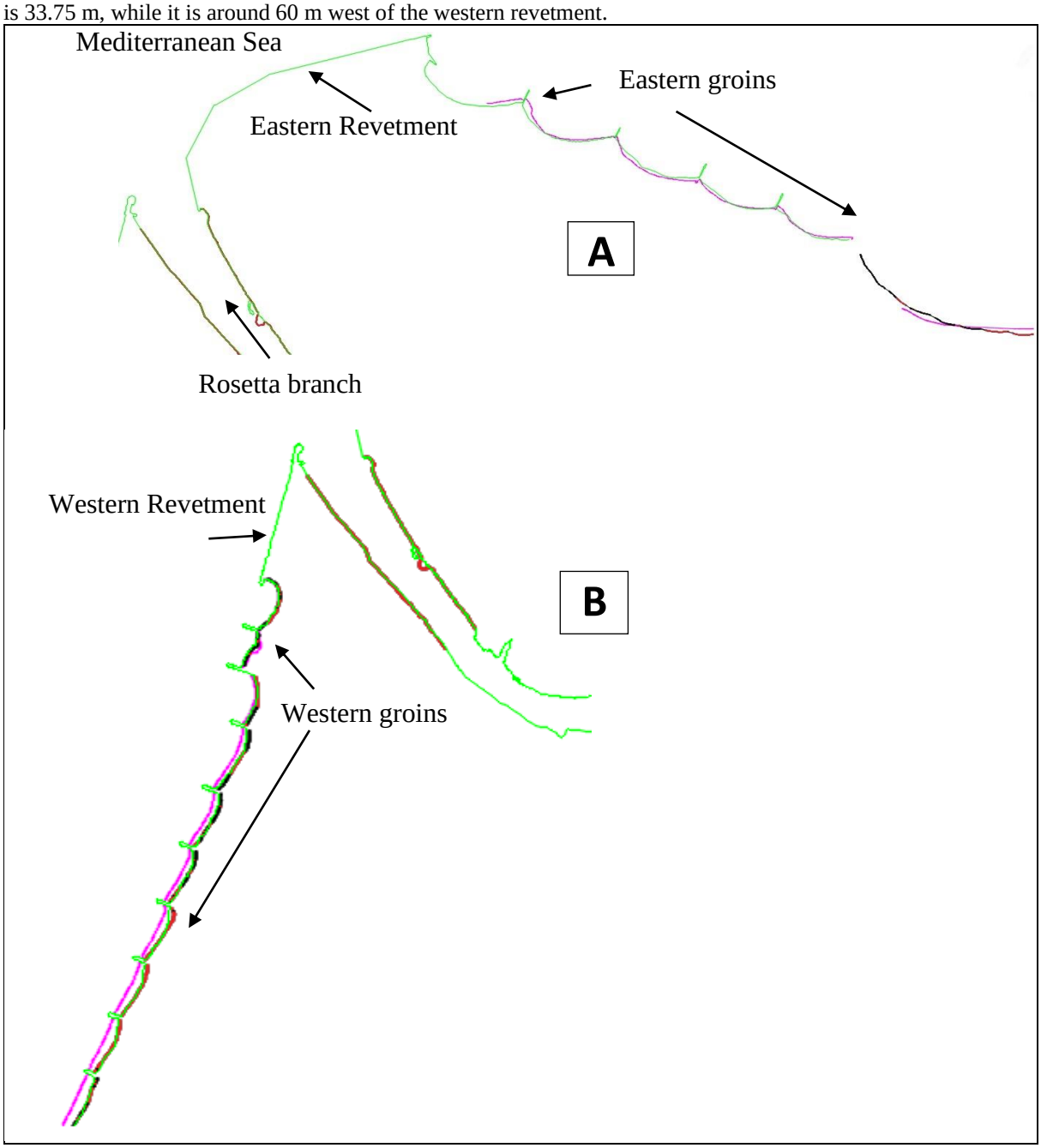

Figure 7. Rosetta Promontory shorelines (November 2016, November 2022, and March 2024): A) for the eastern revetment and five groins; B) for the western revetment and nine groins. groins.

In addition, Figure 8 displays the annual land retreats for the years 1985–2022. The red indicates severe erosion at a rate of 38 m/year, the yellow indicates coastline stability, and the green indicates accretion at a rate of 45.7 m/year. Balbaa, et al. (2020) report that erosion rates on the lee sides of the eastern and western seawalls were around -64 m/y and -20 m/y, respectively, after revetments were installed in 1991. More protection

structures were built as a result in 2005, to the west and east of the respective seawalls. These were the five eastward-facing groins and the nine westward-facing groins of the Rosetta Promontory. These buildings have stopped erosion in its tracks almost entirely, they have also shifted the problem to the structure's flanks.

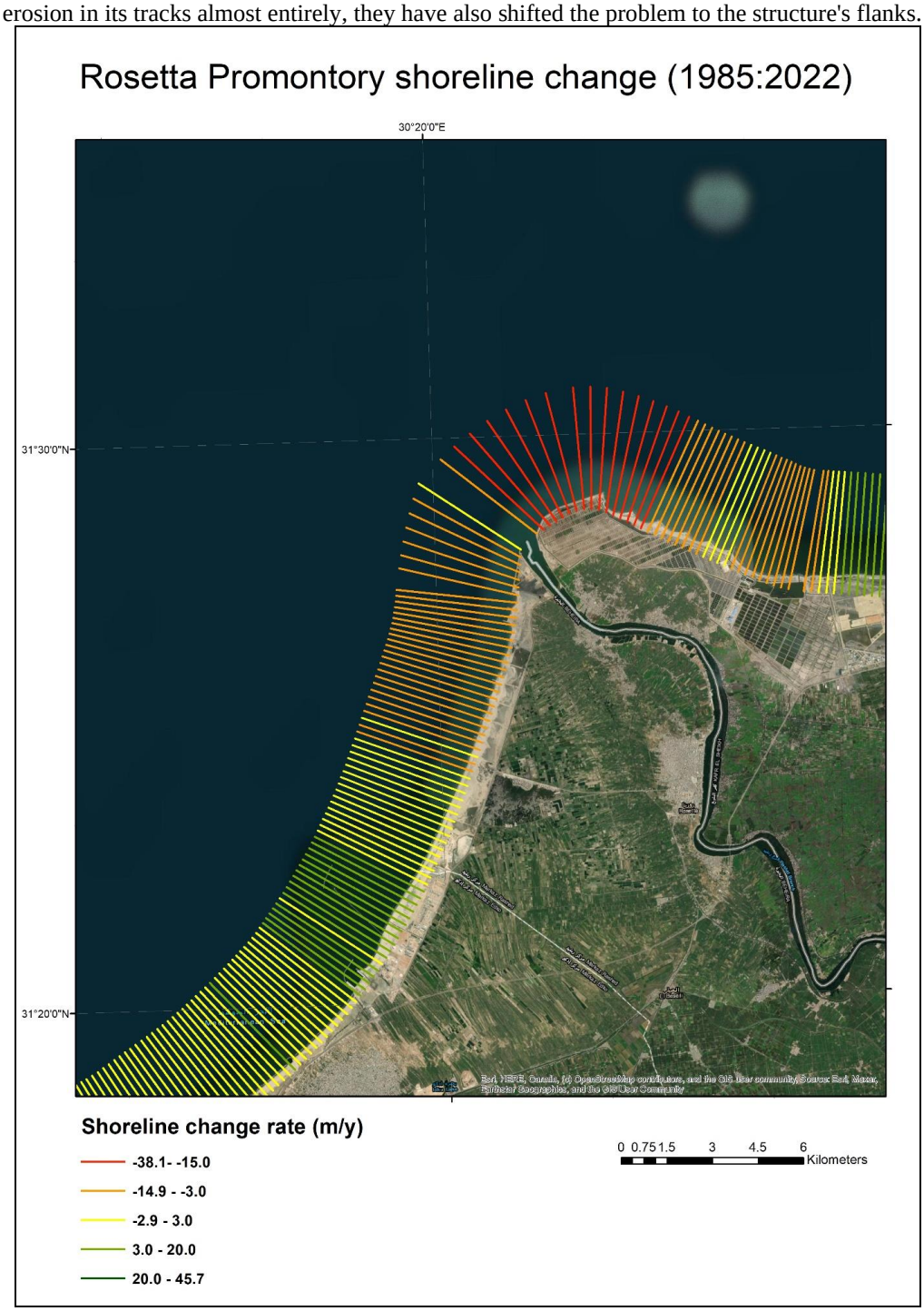

Figure 8. The actual erosion and accretion rates at Rosetta Promontory (1985 to 2022)

3.4 Rosetta Revetment

The Rosetta revetment is 1.5 km long in the east and 3.5 km long in the west. The original design of the Promontory revetment for its trunk and head is shown in Figure 9 (CoRI, 2015). Both Revetment parts are approximately 6 meters above the MSL. The crown of the revetment is 3.3 m wide. Figure 9 shows the level of the sea wall crest (+6.00 m) above MSL and the inclination of the armor layer 1:2.5, as well as the levels of the crest and bottom of the revetment toe, are (-3.50 m) and (-6.0 m) below MSL respectively. In addition, the width of the revetment toe is 12 m. Thus, the beginning of the toe crest of the revetment is about 35 meters from the beginning of the revetment top, and the critical water depth at the toe is (-6.00 m) below MSL.

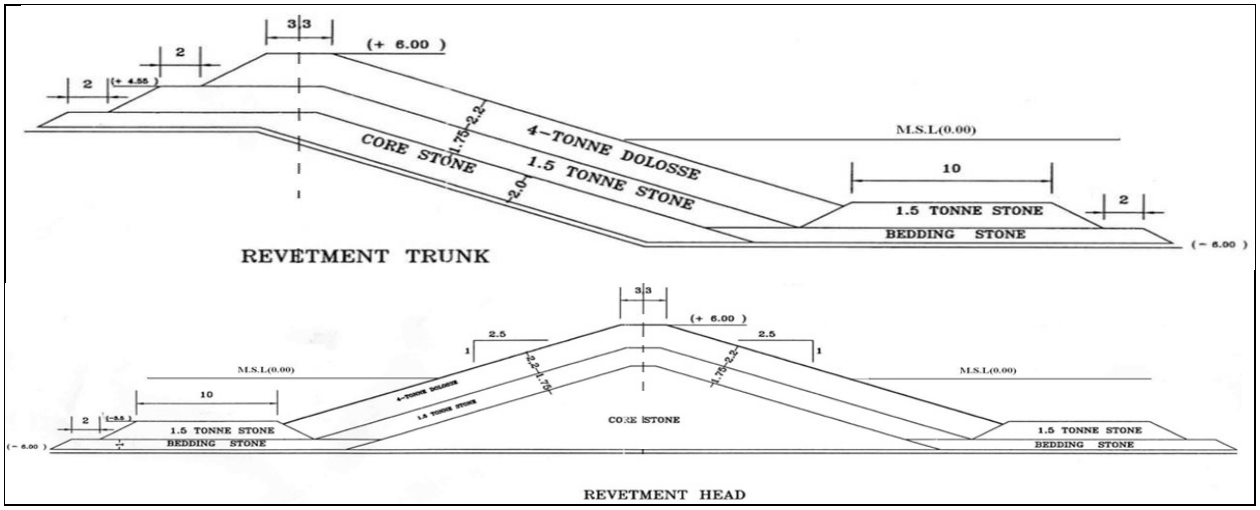

Figure 9. The original design of Promontory revetment for its trunk and head.

3.4.1 The Dolos Blocks

Field investigation revealed that:

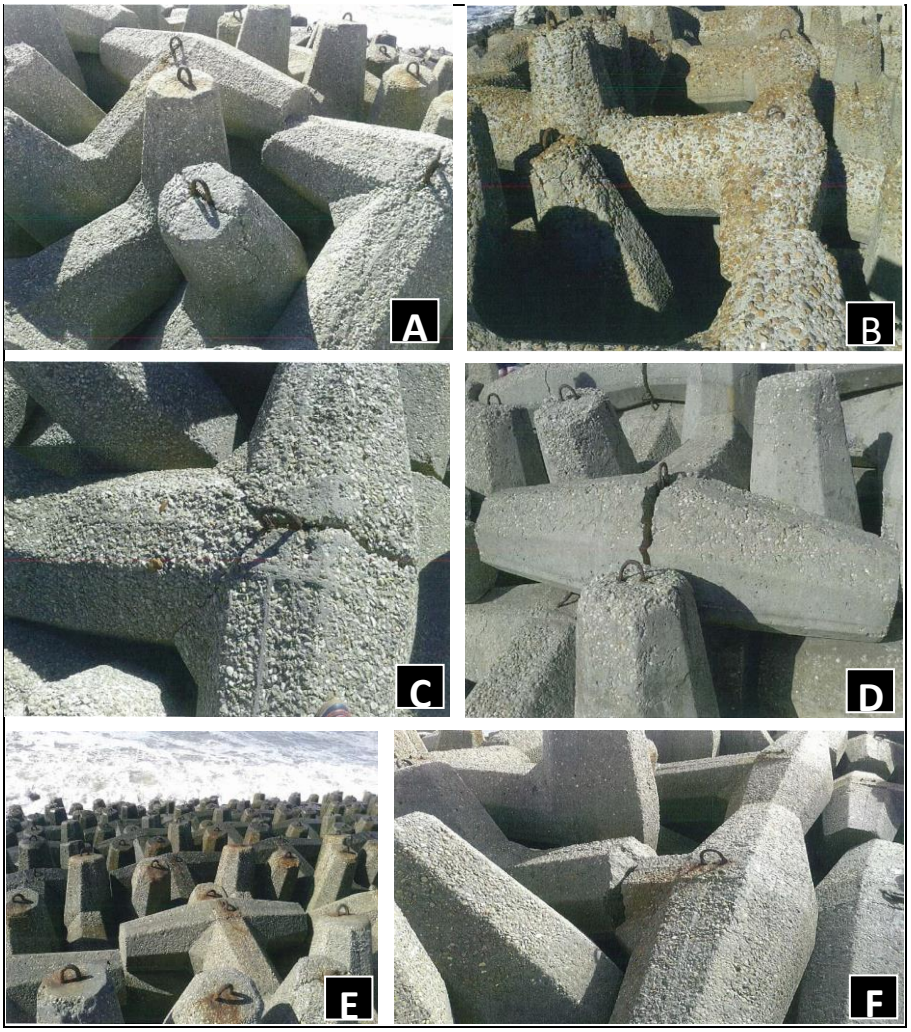

Figure 10. Revetment Dolos: A) Concrete containing fractures Limestone; and B) Concrete containing siliceous gravel; C) Visible cracks due to rusting of steel skewers; D) Complete breakage and separation due to rusting of steel bars; E) Units exposed to waves have a sound outer surface; and F) Fractures in some units flukes away from steel skewers.

- Most Dolos stone units are cast with concrete containing crushed limestone (dolomite), as shown in Figure 10-A, while other units are cast with concrete containing siliceous gravel, as shown in Figure 10-B.
- There is severe rust in the steel skewers used, which resulted in visible and large cracks, especially in the Dolos units located above the water level, as in Figure 10-C.
- The severe rust also caused breakage and complete separation of parts of some Dolos units in the place of the steel skewers or near them, as in Figure 10-D.
- The Dolos units that face directly to the sea and are constantly exposed to waves have a sound surface, do not show any signs of deterioration or corrosion, and do not suffer from the rust of the steel bars, as shown in Figure 10-E. In contrast, the problems of deterioration and steel rust are concentrated in the existing units that are exposed to wave water spray or water vapor, especially in the upper part of them that is directly exposed to the atmosphere, as for the lower part of these units, there are no signs of deterioration.
- Despite the occurrence of deterioration and corrosion on the outer surface of the Dolos units, the cohesion between the large aggregate (limestone fragments or siliceous gravel) and the cement mortar is still strong and no separation has occurred between them.
- There are some Dolos units in which there are fractures away from the steel bars in the onyx area, as shown in Figure 10-F. These units are located on the Western Wall at its meeting with the protection wall on the western mainland of the Rosetta Branch.

3.4.2 The CFD numerical model

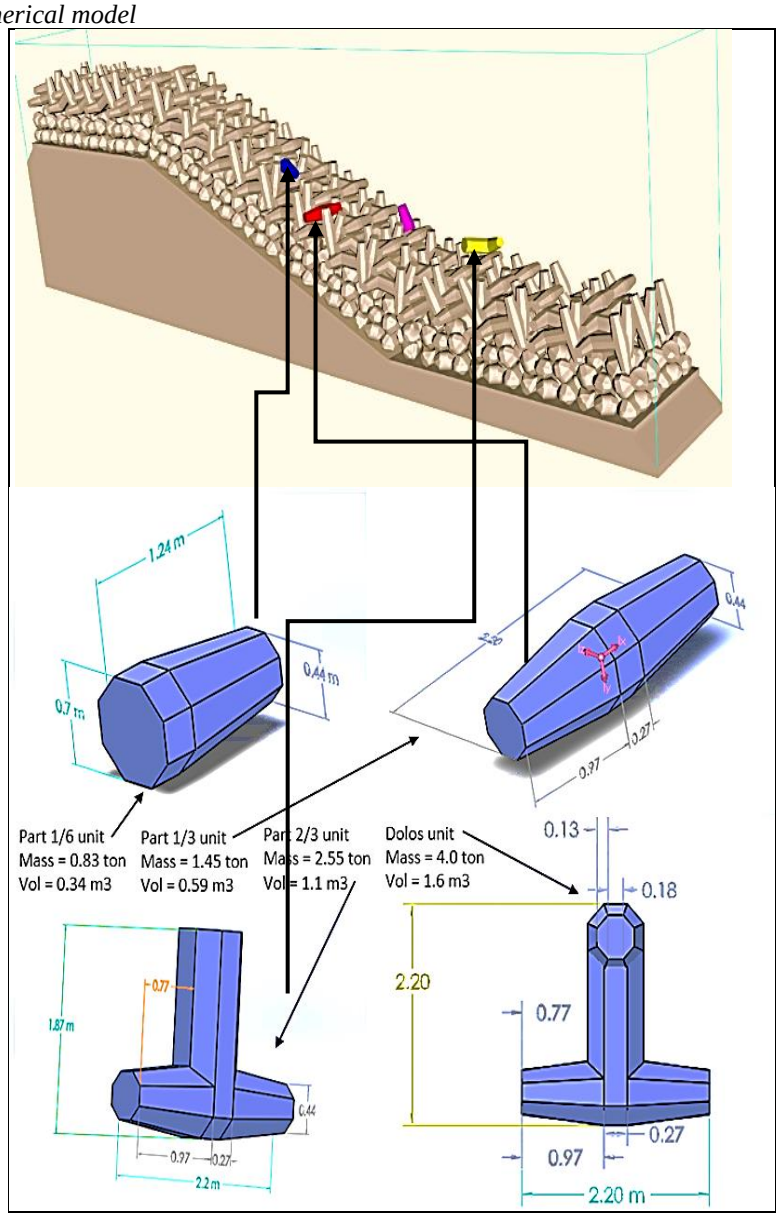

Figure 11. The breakwater and moving units after construction of the STL file.

Fluid structural interaction has been simulated by CFD software (FLOW 3D). Initially, the breakwater was constructed by CAD software by the placement of the individual unit concerning the collision and contact between units. In addition, some broken dolos units were broken and divided into pieces (1/6, 1/3, and 2/3 of the unit) to simulate the collision effect as shown in Figure 11.

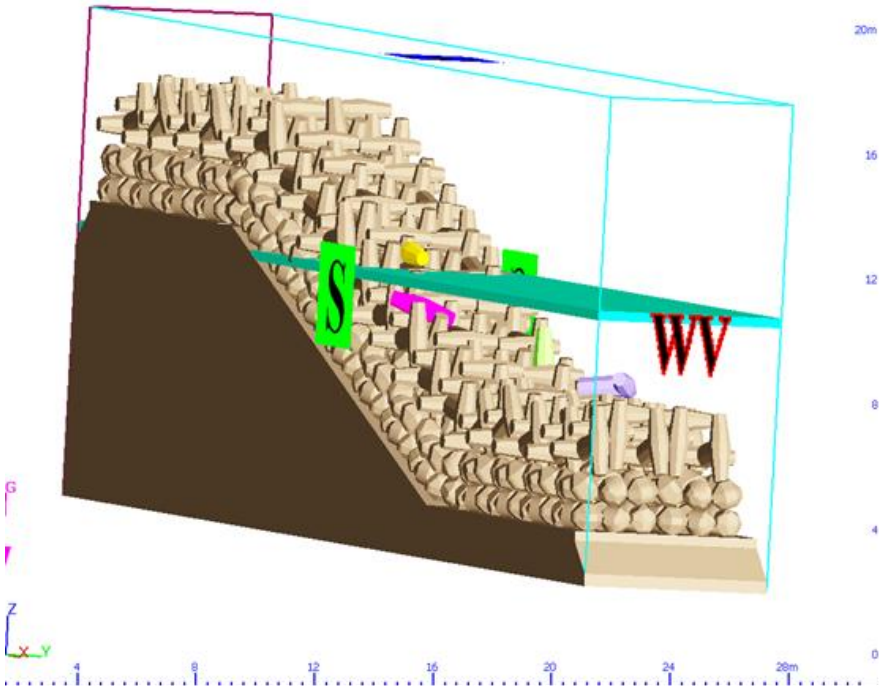

Figure 12. The construction of the revetment and the boundary conditions on FLOW 3D software.

Then, the breakwater was exported to the FLOW 3D as an STL file where a numerical wave flume was set with the dimensions of 50.0 x 6.0 x 6.0 m in the directions of X, Y, and Z, respectively. The domain was divided into cells to solve the fluid equation and evaluate the velocities of the moving parts due to wave loads (Figure 12). The model was used and verified by many researchers (Dentale et al., 2014).

Different mesh sizes have been tested to choose the suitable mesh which consumes time and gives an accurate result. Regarding the CFD simulation, the kinetic energy was closed sometimes because of the scholastic of waves, the used mesh was with 700000 cells of equal size of 0.20 x 0.20 x 0.20 m. The collision model by finite element method gave a good gradual varying because of using specific boundary conditions and loads but it sometimes significantly varied with coarse mesh (0.12 m), the finite element mesh was fine (0.06 m) in the collided zone, and coarse in other zones (Figure 13).

Several experiments have been executed with different water depths and wave heights in front of the Rosetta revetment simulation model. It was found that the ratio between water depth and wave height increased, the greater the moving part velocity, and then greater kinetic energy was given to the moving part. It means that the unit velocity increases with increased wave height and decreases water depth. Also, the maximum wave velocity which is created in the crest part of the wave is more vulnerable to the movement units (Figure 14).

In addition, the moving part's kinetic energy increases with the increase of the wave velocity upon the wave breaking. Also, the water velocity is as high as possible at the wave crest, so the presence of a mass allowed to move in this region enhances the occurrence of collapse (Figure 15).

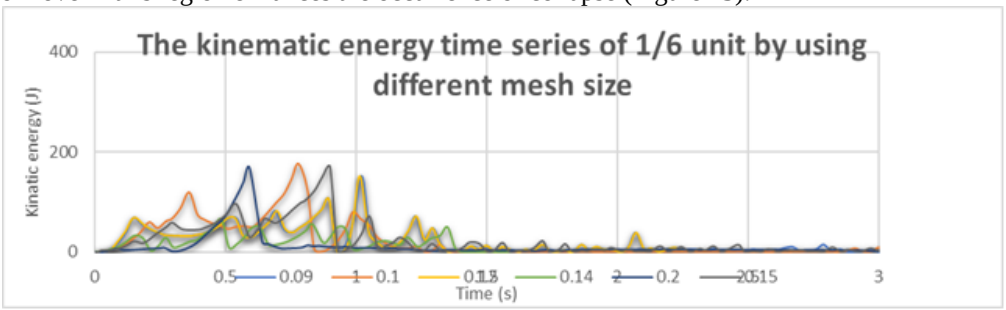

Figure 13. Choosing the mesh size by different mesh comparisons in CFD models.

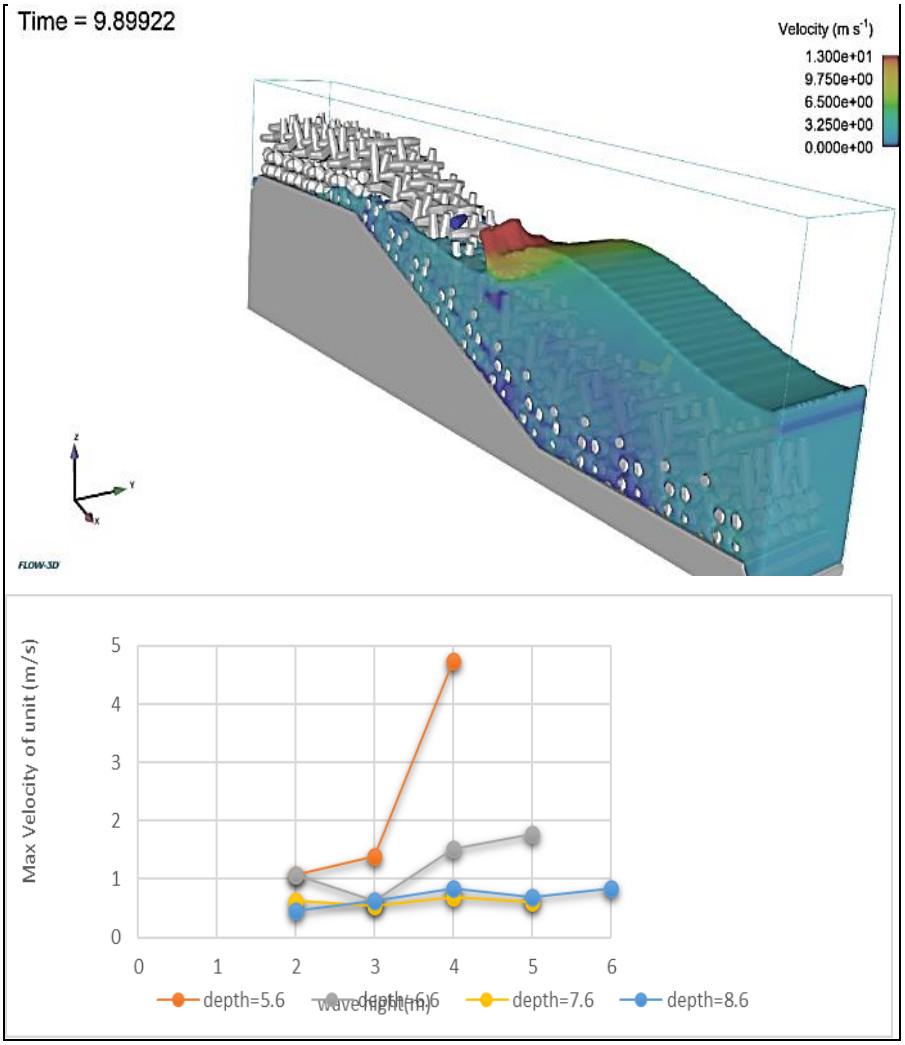

Figure 14. The distribution of wave velocity and the maximum velocity of the moving unit for different flow

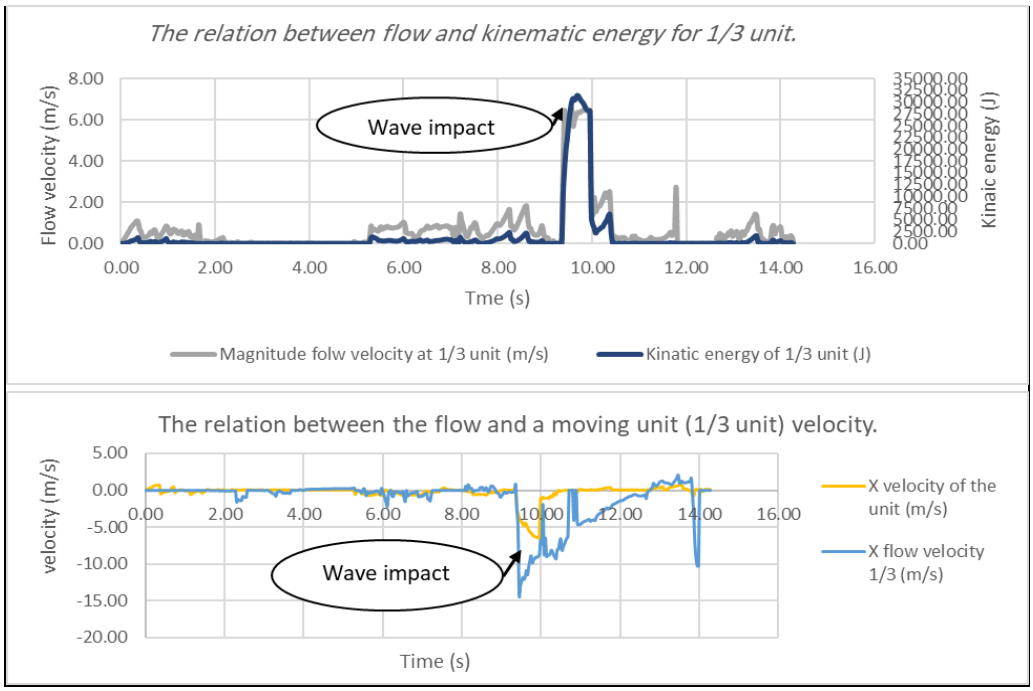

Figure 15. The impact of the flow velocity on a moving unit (1/3 unit) motion.

3.5 Hydrographic Marine Profiles

The location of marine profiles at Rosetta Promontory and the five eastern and nine western groins are illustrated in Figure 16 (CoRI, 2015). The marine profiles extending along the sea wall, which start from the west of the Western Wall in a vertical direction into the sea from Profile No. 1 to Profile No. 7 and then the Eastern Wall from Profile No. 8 to Profile No. 15 (Figure 16), during the period from 2008 to 2015. Through the field investigation of the marine profiles, the variation of sea bed levels from 2008 to 2015 at Rosetta Promontory is illustrated in Figures 17 and 18 (CoRI, 2015). The marine profiles show the relationship between the change in water depth in front of the barrier relative to the MSL and the distance in the seaward direction away from the barrier. The 2015 profiles were surveyed at the beginning of March, and therefore they show the maximum possible erosion that could occur in front of the barrier, as they express the resultant impact of the cores that the place was exposed to from December until February. These profiles indicate the following:

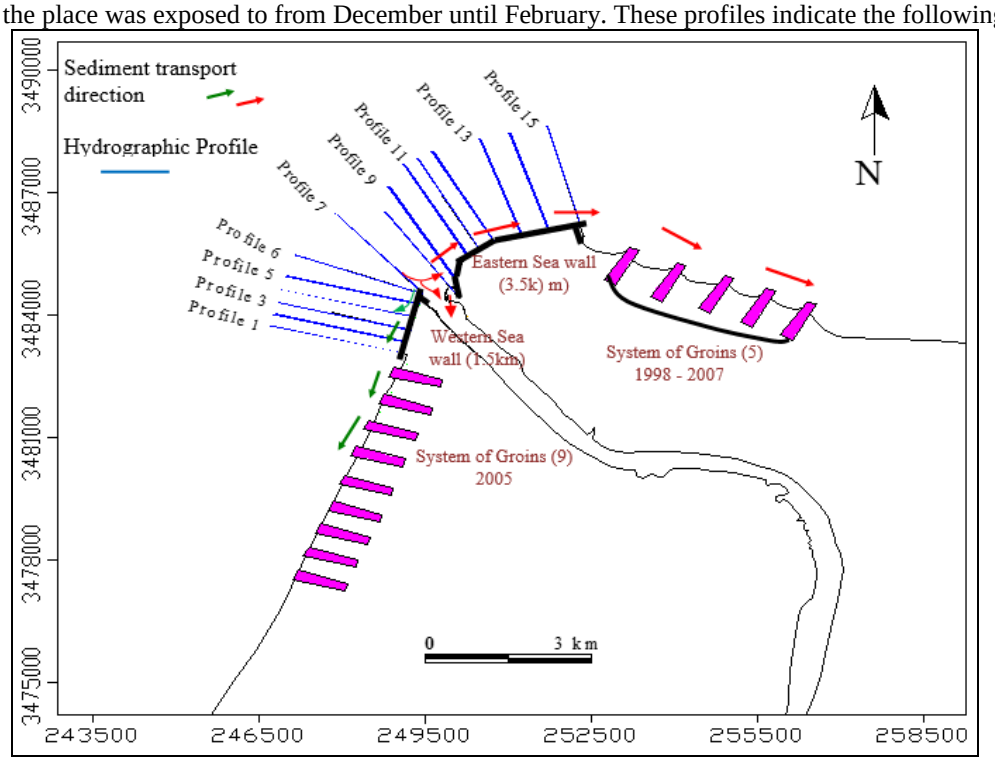

Figure 16. The location of marine profiles at Rosetta Promontory (CoRI, 2015).

- A study of the marine profiles and the sea wall cross-section shows that the toe is covered in all profiles, meaning that the bottom level at the toe is around 3.5 m above MSL. Therefore, the toe of the barrier has not worked yet, knowing that the toe extends from a level of -3.5 m below MSL to a level of -6.00 m below MSL. Therefore, the barrier has not yet operated at its full design capacity, reaching when the bottom level in front of the toe is -6.00 m below MSL.
- For the western barrier, according to the 2015 marine survey (the highest erosion after the storms), the level of sea bed (-6.0 m) below MSL for marine profiles No. 1, No. 2, No. 3, No. 4, No. 5, No. 6, and No. 7, respectively, is located at distances of 350 m, 350 m, 250 m, 250 m, 220 m, 150 m, and 100 m, respectively, measured from the beginning of the toe from the sea side of the profiles, starting from the west to the east. The last two profiles; No. 6 and No. 7, are located at the head of the western barrier towards the mouth of the Nile River, where water emerges at high speeds, causing the highest rate of erosion in these two profiles. By studying the change in profiles over time, all previous profiles are stable.
- For the eastern barrier, the level of sea bed (-6.0 m) below MSL for marine profiles No. 10, No. 11, No. 12, No. 13, No. 14, and No. 15, respectively, are located at distances of 120 m, 120 m, 120 m, 200 m, and 200 m, respectively, measured from the beginning of the toe from the sea side of the profiles starting from the west to the east. The first two profiles; No. 8 and No. 9 are located at the point where the direction of sediment movement changes, as shown in Figure 16. Therefore, they are a source of sediments and are exposed to maximum erosion, which causes increasing depths in these two profiles. By studying the change in profiles over time, all previous profiles are stable.

The results of the profile analysis match the CoRI's studies between 2005 and 2008, and then from 2008 to 2013, as well as, the study that was conducted by the Spanish company ACCIONA at the request of the Ministry of Water Resources and Irrigation (MWRI), which prepared a study on the balance and stability of the

current Rosetta Sea wall. This indicates that the situation has been stable at the checkpoint over the period from 2005 to 2015. The depths in front of the toe of the barrier have not yet reached the critical depth (-6 m) below MSL, which requires intervention with measures to ensure the continued safety and stability of the barrier, knowing that increasing the depth in front of the barrier reduces the rate of erosion. Therefore, there is no danger to the stability of the barrier as a result of erosion and sedimentation operations until 2015.

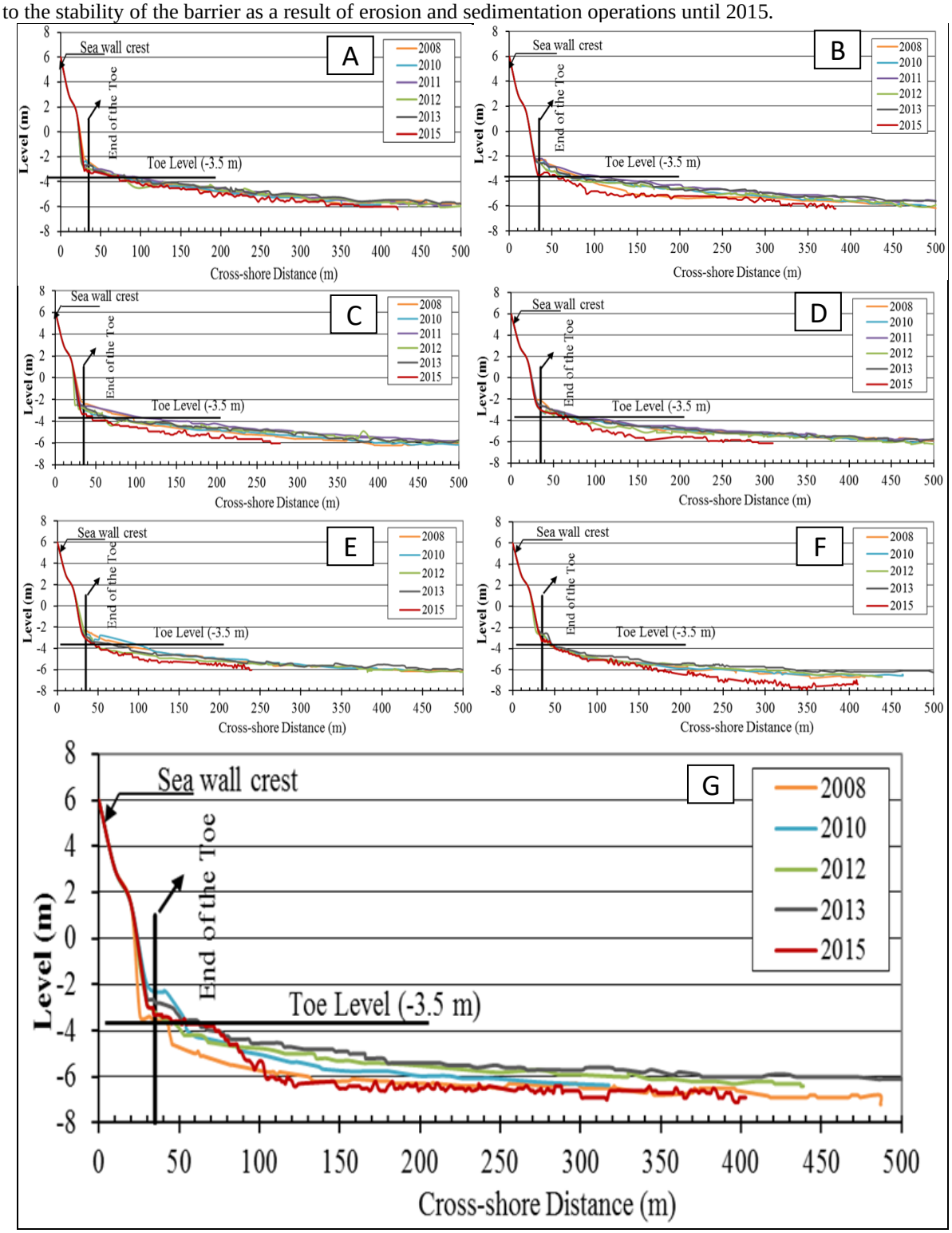

Figure 17. The variation of sea bed levels from 2008 to 2015 at the left part of Rosetta revetment for marine profiles: A) No. 1, B) No. 2, C) No. 3, D) No. 4, E) No. 5, F) No. 6, and G) No. 7 respectively (CoRI, 2015).

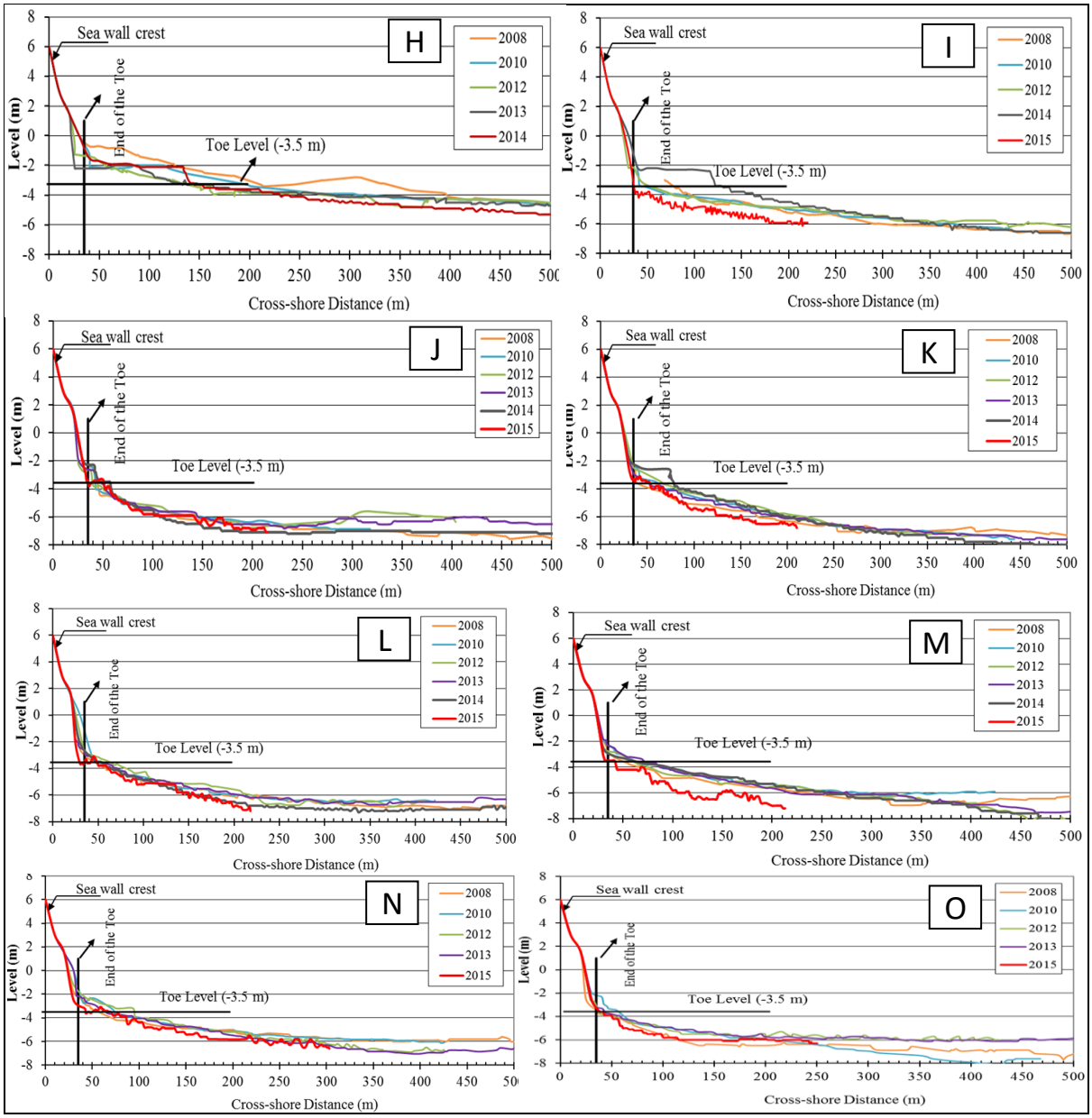

Figure 18. The variation of sea bed levels from 2008 to 2015 at the right part of Rosetta revetment for marine profiles: H) No. 8, I) No. 9, J) No. 10, K) No. 11, L) No. 12, M) No. 13, N) No. 14, and O) No. 15 respectively (CoRI, 2015).

The CoRI carried out a hydrographic marine survey in November 2016, November 2017, November 2020, November 2022, and May 2023 in front of Rosetta Promontory. The hydrographic marine profiles No. 1, and No. 8 for the western revetment, and No. 9, and No. 15 for the eastern revetment are shown in Figure 19 for the years 2016, 2017, 2020, 2022, and 2023. Consequently, the contour map generated for the year 2022, is shown in Figure 20. Figures 14 and 15 show that the sea bed level at the revetment toe varies from (-4.2 m) below MSL at Profile No. 1 west of the western revetment to (-5.30 m) below MSL at Profile No. 8 east of the western revetment and Rosetta branch mouth. This is just less than the critical level (-6.0 m) below MSL, which is level revetment at the bottom. In addition, the sea bed varies from (-2.6 m) below MSL at Profile No. 15 east of the eastern revetment to (-4.20 m) below MSL at Profile No. 9 west of the eastern revetment and Rosetta branch mouth, as shown in Figures 14 and 15. This indicates the critical area is located at the Rosetta branch mouth. That is going to the critical level of the revetment toe (-6.00 m) below MSL as a result of sea level rise due to climate change. Therefore, the main problem is that when the sea bed level reaches (– 8.00 m) below MSL, the toe will be exposed to scouring underneath the revetment toe, leading to failure.

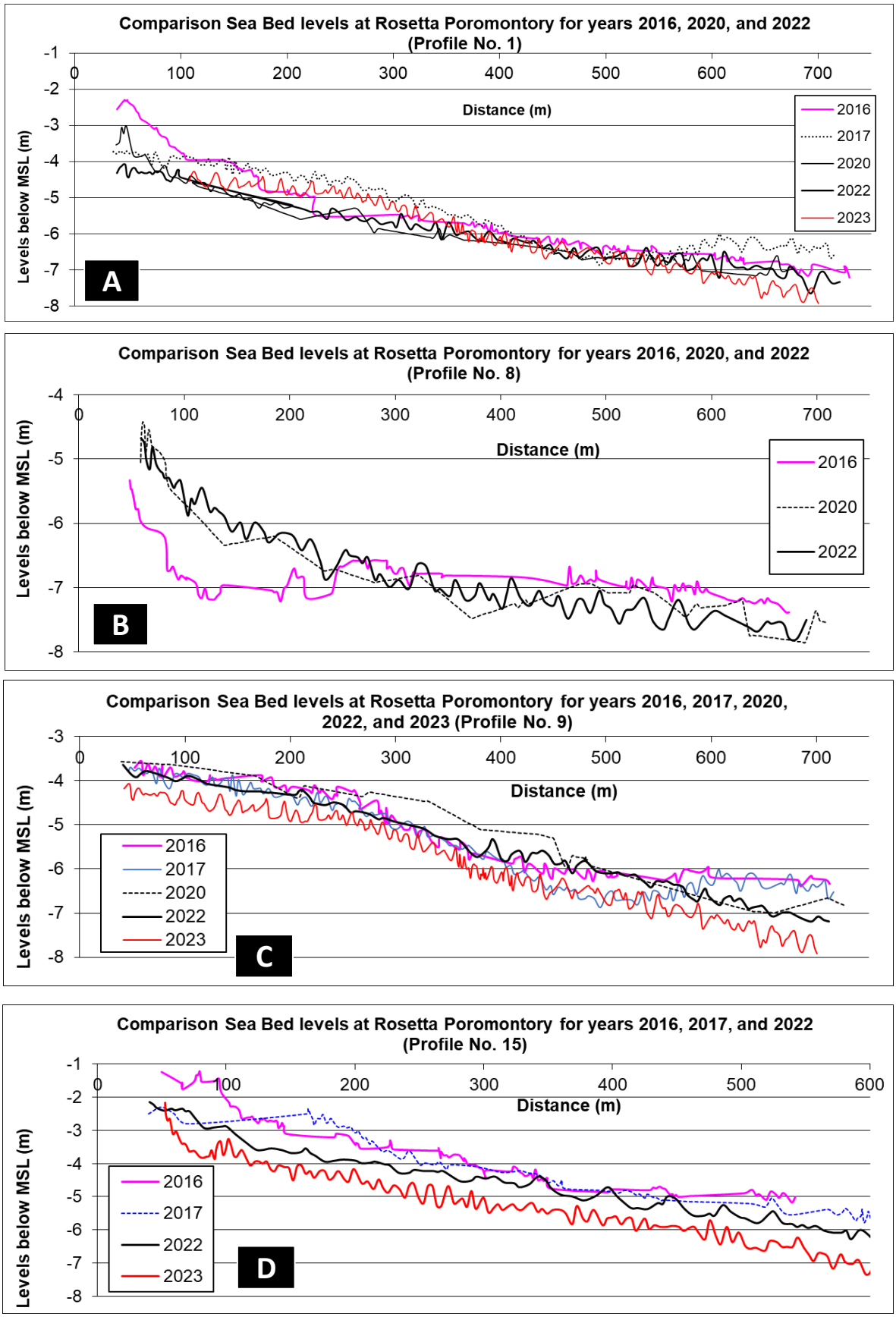

Figure 19. The variation of sea bed levels in 2016, 2017, 2020, 2022, and 2023 at the right part of Rosetta revetment for marine profiles: C) No. 9; and D) No. 15.

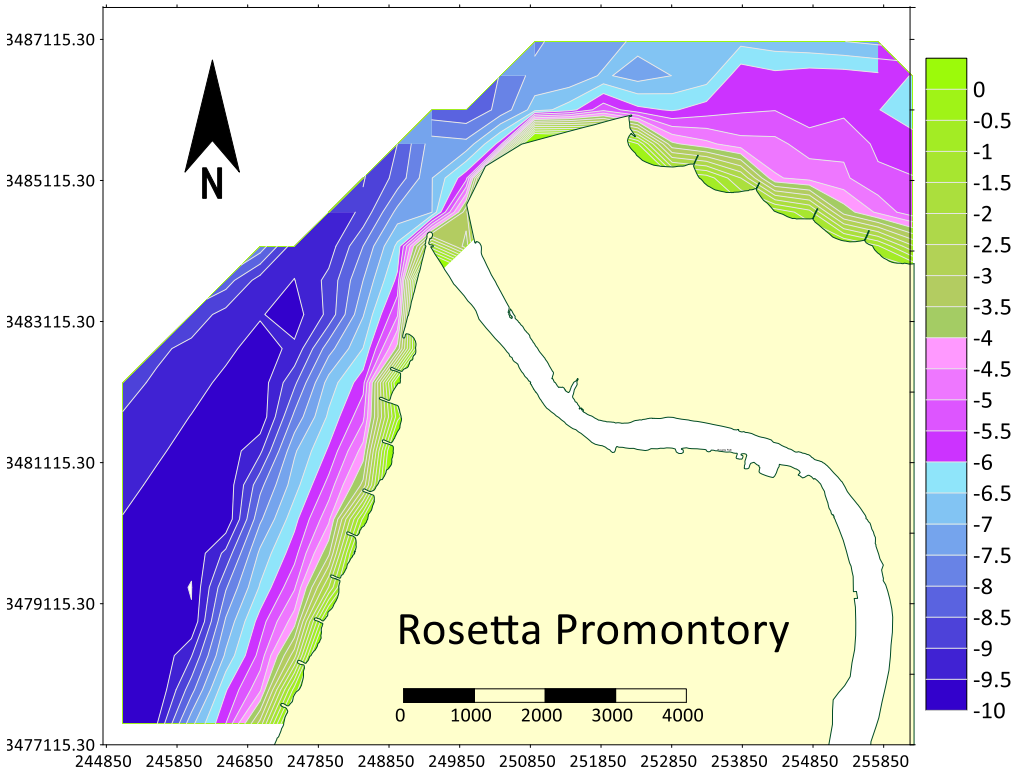

Figure 20. The contour map of the area study in 2022.

3.5.1 The Spanish company ACCIONA Study

The Spanish company ACCIONA, at the request of the Ministry of Water Resources and Irrigation, had previously prepared a study on the balance and stability of the current sea wall using physical models once the depth of the water in front of the toe of the current wall reached (-6.0 m) and (-8.0 m) below MSL, as well as studying three structural alternatives to protect the current sea wall: One of them is to deepen the foundation level of the toe of the sea wall to (-8.0 m) below MSL while increasing the length of the toe. The other two are to create a submerged barrier in front of the current sea wall with a water depth above its crest - 0.5 m or -1.2 m.

The results of studies of physical models indicated that no significant damage occurred in the protective toe layer in all laboratory tests that were conducted and that the only damage occurring in the protection sector arose in the armor layer of the dolos units, and this is due to the lack of supporting of the last row of the armor layer in the backside, which makes the current sector unstable and vulnerable to destruction when water immersion occurs over the current protection sector, especially with the scenario of a sea level rise of +2 m. To avoid this problem, the study recommended strengthening the armor layer of the current wall from the back. The effectiveness of this recommendation was confirmed by additional tests in which the armor layer was reinforced on the back side of the current sector by increasing the width of the crown to 7.3 m and filling the area between the (+ 2.8 m) above MSL to (+ 6.75 m) above MSL levels with stones weighing 1.5 tons. The tests confirmed the stability and balance of the sector. The current situation after consolidation in the face of the water depths in front of it reaching (-6 m) below MSL, as well as (-8 m) below MSL without or with the use of the proposed alternatives with the current protection with the sea level rising to (+2.0 m) above MSL, as none of the dolos units moved. The study revealed that there were no significant damages to the protective toe layer in all laboratory tests conducted. All tests were conducted on units weighing 4 tons, which are not exposed to any damage or breakage, which does not represent the true state of protection at present. Considering that the Dolos units are artificial, their efficiency lies in the interlocking between the units, which means the possibility of weakness of the sector and possible problems in its stability and balance. Therefore, the study concluded that all previous results of strengthening the sector or the proposed alternatives will not be sufficient to ensure the balance and stability of the current sector unless the broken and damaged Dolos units in the current sector are first replaced for protection. However, two problems appear on the horizon that must be considered. The first is to avoid the occurrence of scouring in front of the toe of the wall when the water level in front of the toe begins to reach the foundation depth of (-6.0 m) below MSL. The second is the fractures and damage (Figure 10-D and Figure 10-F) that currently exist in some Dolos units in the armor layer (artificial Dolos units are represented by their efficiency in interlocking units), the effect of which was not taken into account when using physical models.

3.6 Spectral Wave Model

The wave climate within the computational domain is established using the MIKE 21 SW model. The wave model has been used to generate a continuous wave parameter over the whole study area for 1 year (2022), as shown in Figure 21. The wave height at the groins varied between 0.25 to 0.5 m. This indicates that the coastal protection structures aid in reducing the wave stresses between the Groins. MIKE 21 Spectral Wave Model (SW) is a 3rd generation time-dependent spectral wind-wave model based on flexible meshes. It stimulates the growth, propagation, decay, and transformation of wind-generated waves and swells in offshore and coastal areas. The model includes the effects of wave growth by the action of wind, the interaction between waves with different frequencies, and dissipation due to white capping. Furthermore, the model includes shallow water effects like diffraction, refraction, and shoaling due to varying depth and dissipation due to depth-limited wave breaking and bottom friction.

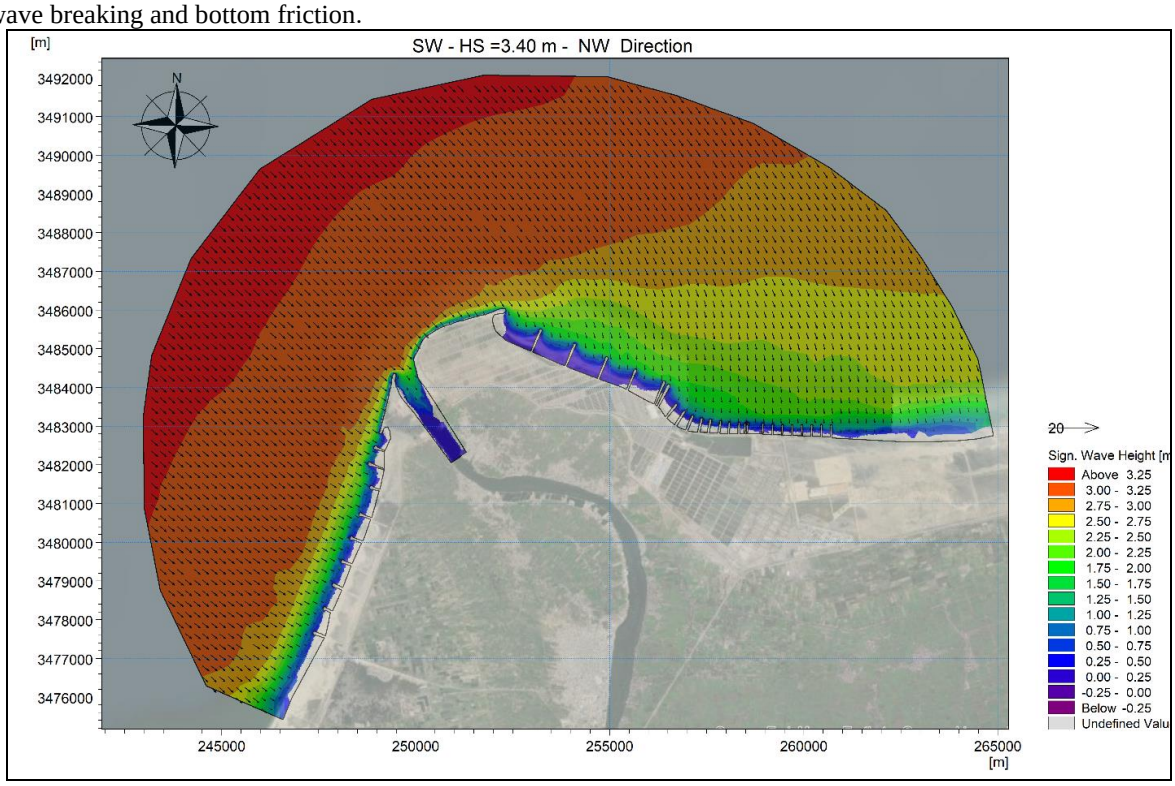

Figure 21. Spectral Wave Model Results for significant wave height.

3-7 Hydrodynamic Model

Figure 22 shows the current velocity in the study area. It is varied from 0.533 to 0.933 m/sec.

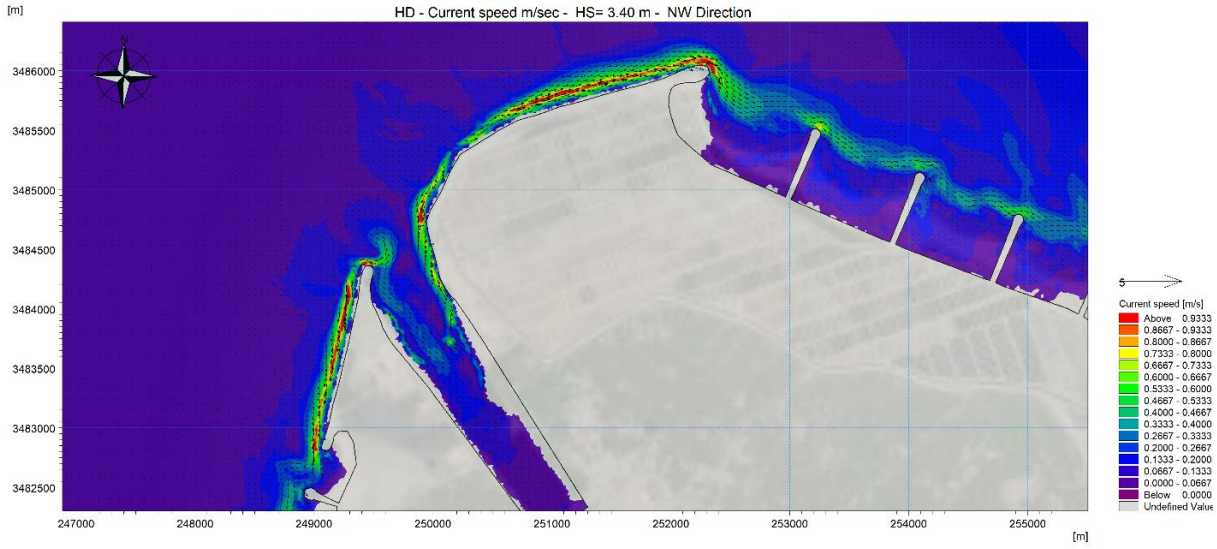

Figure 22. Hydrodynamic Model Results for current velocity m/sec.

3.7 The last deterioration of the Rosetta Sea wall

At the eastern revetment of the Rosetta promontory in Dec 2022, some units of the armor layer had broken and fallen to the toe in two locations, leading to the exposure of the basalt layer located below the armor layer. Figure 23 illustrates the location of the last deterioration of the Rosetta Eastern Revetment that occurred in 2022. The principal factor contributing to these collapses is the wall's natural morphology or the orientation of the sea wall relative to the direction of the most frequent waves. This is mostly caused by the wall's uneven straightness, which indicates that the directions of the sea currents in these areas vary. At the base of the wall, erosion is accelerated by this current divergence, which makes erosion worse. Because different directional forces are acting on the structure as a result of the currents diverging, erosion is intensified and accelerated. Figure 24 shows the multi-directional current at the location of the eastern seawall deterioration.

Turbulent flow patterns are produced by diverging currents interacting along the surface of the wall. Asymmetrical erosive forces are caused by the varied pressures that these turbulent flows apply to the wall's various parts. Therefore, sections that are next to places where currents are diverging may experience relatively less erosion, whereas areas where currents are converging may experience increasing erosion rates. Differential erosion increases the risk of collapses or failures in various areas by weakening the wall's structural integrity, especially near its base.

Figure 23. The last deterioration of the Rosetta Eastern Sea wall occurred in 2022.

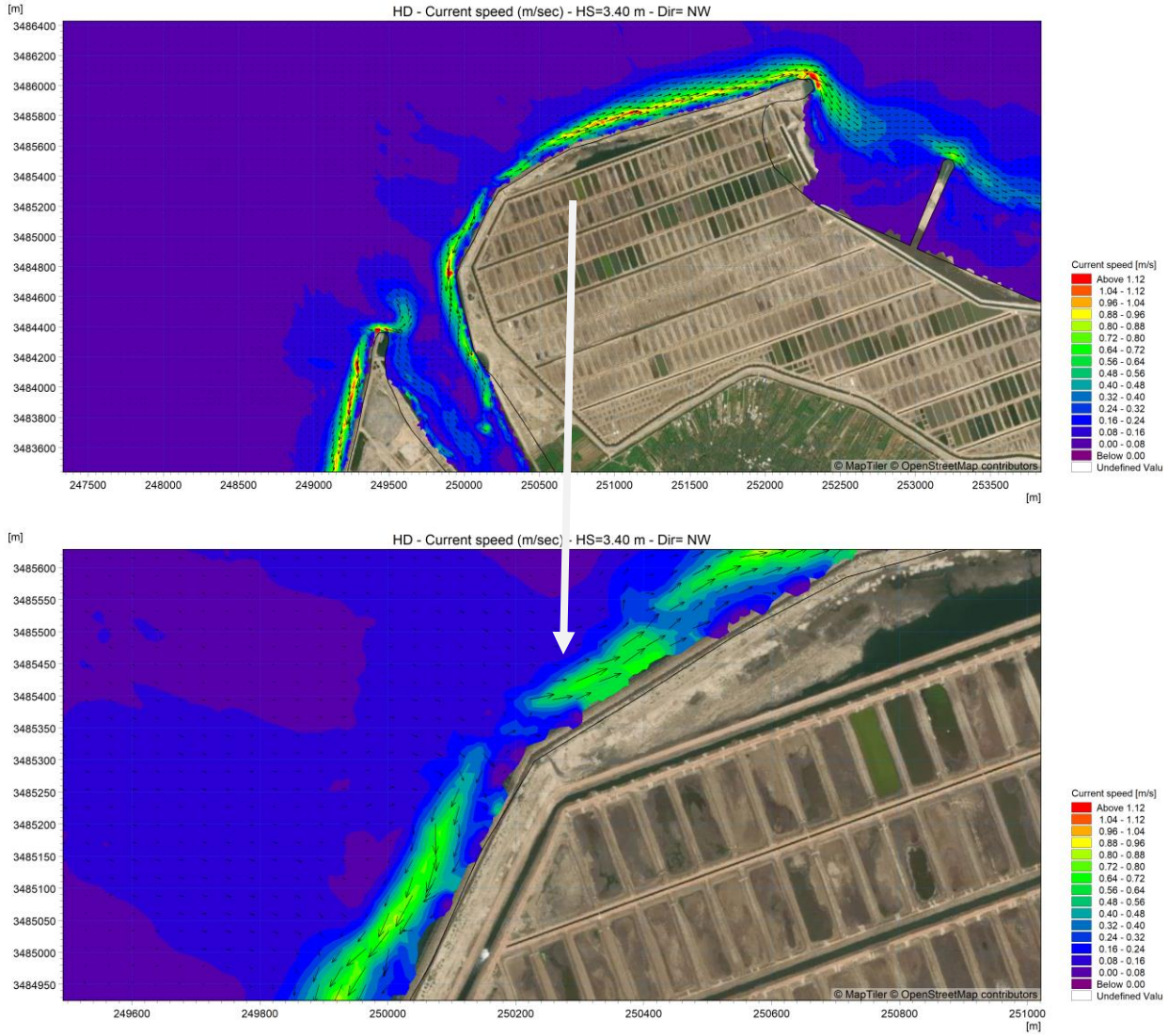

Figure 24. The multi-directional current at the location of the eastern seawall deterioration.

IV. CONCLUSIONS AND RECOMMENDATIONS

The coast of the Nile Delta has been suffering extensive accretion and erosion problems. As a result of sea level rise due to climate change, low-lying regions of the Nile Delta are experiencing flooding. Rosetta Promontory is considered one of the most erosional areas on the Nile Delta coast. The Rosetta Revetment was constructed during the period from 1986 to 1991 with two sides. Following the two revetments' completion, the land and shoreline were successfully prevented from retreating. However, after 2000, erosion occurred alongshore on the western and eastern sides, respectively. Consequently, the eastern revetment was extended by approximately 250 meters. To slow down the rate of erosion, 15 groins were constructed between 2003 and 2005 on both the eastern and western sides of the Rosetta Promontory Sea walls. Of these, five rubble mound groins with a length of 400 to 500 m and a spacing of 800 to 900 m were built to safeguard the eastern side. During the period from 2008 to 2015, the revetment was nearly stable except for the area surrounding the Rosetta branch mouth at the head of the western and eastern barrier, where water emerges at high speeds, causing the highest rate of erosion. In 2024, despite all the protective measures taken, the Rosetta promontory continues to face erosion and sedimentation issues. As a result, the main problems in Rosetta revetments are the structure deterioration, as well as, the lack of structural functions. This is because of fractures and damage to some Dolos units of protective shield layers. This leads to minimizing its interlocking, leading to hydraulic instability and failure in the future. In addition to the bottom erosion in front of the revetment, the erosion processes migrated to both RP sides, east of the eastern and west of the western revetments. Furthermore, the Rosetta branch experiences sedimentation issues that impact the fish boats' navigation. Consequently, the Shore Protection Authority repaired the eastern head of the western revetment in 2019. The repair spanned roughly 350 meters from the start of the western revetment and involved replacing two rows of the shattered Dolos along

the crest with the same weight (4.0 tons), in addition, to constructing a new revetment in front of the current one. The cross-section of the new revetment was composed of 6-ton tetrapod units for the armor layer, 2-3-ton dolomite stones for the toe layer, 500–1000 kg of stones for the underlayer, and 10-200 kg of weight stones for the core. The project costs roughly 64.429 million Egyptian pounds. From the shoreline positions for the years 1985 to 2022, the annual rate of erosion at the eastern side of the Rosetta revetment is 38 m/year. Recently, the sea bed level at the revetment toe has varied from (-4.2 m) below MSL at the west of the western revetment to (-5.30 m) below MSL at the east of the western revetment and Rosetta branch mouth. This is just less than the critical level of the revetment toe bottom (-6.00 m) below MSL. In addition, the sea bed varies from (-2.6 m) below MSL at the east of the eastern revetment to (-4.20 m) below MSL at the west of the eastern revetment and Rosetta branch mouth. This indicates the critical area is located at the Rosetta branch mouth. Sea level rise leads to the sea bed level is going to reach the critical level of the revetment toe underneath the toe foundation (-6.00 m) below MSL. Consequently, it will be exposed to scouring, leading to failure. Therefore, the study recommends building a submerged breakwater in front of the existing sea wall with a water depth of 0.5 meters above its crest to absorb wave energy, as well as deepening the foundation level of the revetment toe to (-8.00) meters below MSL and expanding it by 10 meters. This is to overcome the expected dangerous state due to sea level rise. In addition, the study recommends the construction of two jetties at the mouth of the Rosetta branch to protect it from sedimentation and enhance navigation. This proposed solution needs verification through mathematical models.

Acknowledgments

The author would like to thank the marine staff of Rosetta Coastal Research Station for their contributions to the field activities of the study. The author also appreciates the help of Ibrahim M. Abdelmenem in running FLOW 3D software, in addition, to Ahmed Elsotohy in running Mike Zero software.

References

[1]. Abd-Elmonem, Ibrahim M., Abedio, Tarek I., Kheireldin, Khaled A. Soliman, Mohammed R. (2022). Assessment of Coastal Revetment: A case study of Rosetta Revetment. Ain Shams Engineering Journal 13 (2022) 101623.

[2]. Aly M. H., Giardino J. R., Klein A. G. and Zebker H. A. (2012). InSAR study of shoreline change along the Damietta Promontory, Egypt. Journal of Coastal Research, 284(May), 1263–1269. https://doi.org/10.2112/JCOASTRES-D-11-00182.1.

[3]. Andersen, T. L. (2006). Hydraulic Response of Rubble Mound Breakwaters. December, 429.

[4]. Balbaa, Sherif H., El-Gamal, Ayman A., Mansour, Ahmed S. and Rashed, Mohamed A. (2020). Mapping and Monitoring of Rosetta Promontory Shoreline Pattern Change, Egypt. Journal of Oceanography & Marine Environmental System 4 (2): 29-42, 2020.

[5]. Campos Á, Castillo C, Molina-Sanchez R. (2020). Damage in Rubble Mound Breakwaters. Part I: Historical Review of Damage Models. Journal of Marine Science and Engineering 2020;8(5):317. doi: https://doi.org/10.3390/jmse8050317.

[6]. Ciria, Cur, and Cetmef. (2007). Design of marine structures. The Rock Manual, The Use of Rock in Hydraulic Engineering, 773–907.

[7]. Coastal Research Institute (CoRI). (2004). Technical report on waves at Idku Region. Internal Technical Report, Coastal Research Institute, Alexandria, Egypt.

[8]. Coastal Research Institute (CoRI). (2015). Technical report on Rosetta Promontory. Internal Technical Report, Coastal Research Institute, Alexandria, Egypt.

[9]. Coastal Research Institute (CoRI). (2016). Technical report on sea level variation at Rosetta City from January 2015 to January 2016. Internal Technical Report, Coastal Research Institute, Alexandria, Egypt.

[10]. CoRI/UNESCO/UNDP. (1978). Coastal Protection Studies, Final Technical Report.

[11]. Deabes E. (2017). Applying ArcGIS to Estimate the Rates of Shoreline and Back-Shore Area Changes along the Nile Delta Coast, Egypt. International Journal of Geosciences, 8, 332–348. https://doi.org/10.4236/ijg.2017.83017.

[12]. Deltares. (2017). Tools for a preliminary assessment of coastal problems and solutions. 767–772.Dewidar K. M. and Frihy O. E. (2010). Automated techniques for quantification of beach change rates using Landsat series along the North-eastern Nile Delta, Egypt. Journal of Oceanography and Marine Science, 1, 28–39.

[13]. Dentale, F., Donnarumma, G., & Carratelli, E. P. (2014). Rubble mound breakwater: Run-up, reflection, and overtopping by numerical 3D simulation. Coasts, Marine Structures and Breakwaters 2013: From Sea to Shore - Meeting the Challenges of the Sea, 2, 1164–1173.

[14]. Dewidar K. M. and Frihy O. E. (2010). Automated techniques for quantification of beach change rates using Landsat series along the North-eastern Nile Delta, Egypt. Journal of Oceanography and Marine Science, 1, 28–39.

[15]. El Banna M. M. (2007). Erosion and accretion rates and their associated sediment characters along Ras El Bar coast, northeast Nile Delta, Egypt. Environmental Geology, 52(1), 41–49. https://doi.org/10.1007/s00254-006-0447-2.

[16]. El Sayed W. R., Aly M. A. Iskander M. M. and Fanos A. M. (2007). Evolution of Rosetta Promontory during the last 500 years, Nile Delta coast, Egypt. Eighth International Conference on the Mediterranean Coastal Environment, MEDCOAST 07, 2, 1003–1015.

[17]. El-Asmar H. M. and White K. (2002). Changes in coastal sediment transport processes due to construction of New Damietta Harbour, Nile Delta, Egypt. Coastal Engineering, 46, 127.

[18]. El-Gamal A. (2012). A new approach for erosion and accretion coasts discrimination. Journal of Coastal Research, 389–398. https://doi.org/10.2112/JCOASTRES-D-10-00154.1

[19]. Elsayed M. A. K. and Mahmoud S. (2007). Groins system for shoreline stabilization on the east side of the Rosetta Promontory, Nile Delta coast. Journal of Coastal Research, 23(2), 380–387. https://doi.org/10.2112/04-0319.1

[20]. Fanos A. M. (1999). Problems and protection work along the Nile Delta coastal zone. Fifth International Conference on Coastal and Port Engineering in Developing Countries.

[21]. Fanos A. M., Khafagy A. A., and Dean R. G. (1995). Protective works on the Nile Delta coast. Journal of Coastal Research, 11(2), 516–528.

[22]. Flow Science. (2009). User Manual: FLOW-3D® Cast 3.2. 1–49. https://doi.org/10.1007/SpringerReference_28001
[23]. Frihy O. E., Debes E. A., and El Sayed W. R. (2003). Processes reshaping the Nile delta promontories of Egypt: pre- and post-protection. Journal of Geomorphology, 53(3), 263–279. https://doi.org/10.1016/S0169-555X(02)00318-5.
[24]. Frihy O. E., El Banna M. M., and El Kolfat A. I. (2004). Environmental impacts of Baltim and Ras El Bar shore-parallel breakwater systems on the Nile delta littoral zone, Egypt. Environmental Geology, 45(3), 381–390. https://doi.org/10.1007/s0054-003-0886-y
[25]. Frihy O. E., Fanos A. M., Khafagy A. A., and Komar, P. D. (1991). Nearshore sediment transport patterns along the Nile Delta Egypt. Journal of Coastal Engineering, 15, 409.
[26]. Frihy O. E., Shereet S. M., and El Banna M. M. (2008). Pattern of beach erosion and scour depth along the Rosetta Promontory and their effect on the existing protection works, Nile Delta, Egypt. Journal of Coastal Research, 24((4)), 857.
[27]. Frihy OE, Deabes EA. (2011). Beach and nearshore morphodynamics of the central bulge of the Nile Delta coast, Egypt. International Journal of Environmental Protection, Vol.1 No.2 2011 pp. 33-46. www.ijep.org © World Academic Publishing.
[28]. Frihy, O. E., & Komar, P. D. (1993). Long-term shoreline changes and the concentration of heavy minerals in beach sands of the Nile Delta, Egypt. In Marine Geology (Vol. 115). https://doi.org/10.1016/0025-3227(93)90054-Y.
[29]. Ghoneim E. (2009). A Remote Sensing Study of Some Impacts of Global Warming on the Arab Region. Climate Change: The Arab Forum for Environment and Development (AFED).
[30]. Ghoneim E., Mashaly J., Gamble D., Halls J., and AbuBakr M. (2015). Nile Delta exhibited a spatial reversal in the rates of shoreline retreat on the Rosetta promontory comparing pre- and post-beach protection. Geomorphology, 228, 1–14. https://doi.org/10.1016/j.geomorph.2014.08.021.
[31]. Guo L., Latham, JP, Xiang, J. (2015). Numerical simulation of breakages of concrete armor units using a three-dimensional fracture model in the context of the combined finite-discrete element method. Comput Struct 2015;146:117–42. doi https://doi.org/10.1016/j.compstruc.2014.09.001.
[32]. Hassanin, A. and Jukes, P. (2018). Inspection, Monitoring, Maintenance, and Repair. Encyclopedia of Maritime and Offshore Engineering 2018;1–10. Doi: https://doi.org/10.1002/9781118476406.emoe563.
[33]. Himmelstoss, E. A., Henderson, R. E., Kratzmann, M. G., & Farris, A. S. (2018). Digital Shoreline Analysis System (DSAS) version 5.0 user guide. In Open-File Report. https://doi.org/10.3133/ofr20181179.
[34]. Ibrion M, Paltrinieri N, Nejad AR. (2020). Learning from failures: Accidents of marine structures on Norwegian continental shelf over 40 years time period. Eng Fail Anal 2020;111. doi https://doi.org/10.1016/j.engfailanal.2020.104487.
[35]. Maddrell, R. (2006). Lessons Re-learnt from the failure of marine structures. International Conference on Coastlines, Structures, and Breakwaters 2005: Harmonising Scale and Detail - Proceedings of the International Conference on Coastlines, Structures and Breakwaters 2005, 2006, 139–152.
[36]. Melby JA. (1993). Dolos design procedure based on Crescent City prototype data. Technical Report - US Army Coastal Engineering Research Center 1993;93 – 10 (June).
[37]. Mitsui, J., Yamamoto, M., Noboru, S., & Nishiwaki, I. (2010). Impact force analysis on wave dissipating concrete blocks during rocking motion. Proceedings of the Coastal Engineering Conference, 2–7.
[38]. Muttray, M, Reedijk, B. (2008). Design of Concrete Armor Layers. Ocean Coast Manag. 2008; October:1–17.
[39]. Myrick, G. B., & Melby, J. A. (2005). Monitoring of Dolos Armor Units at Crescent City, California Monitoring of Dolos Armor Units at Crescent City, California. September.
[40]. Najafi-Jilani, A., Zakiri Niri, M., & Naderi, N. (2014). Simulating three-dimensional wave run-up over breakwaters covered by antifer units. *International Journal of Naval Architecture and Ocean Engineering*, *6(2)*, 297–306. https://doi.org/10.2478/IJNAOE-2013-0180
[41]. Oliver J, Plotkin D, Pirie D, Lesnik J. (1998). Condition and Performance Rating Procedures for Rubble Breakwaters and Jetties. US Army Corps of Engineers Construction Engineering Research 1998. Laboratories.
[42]. Pedro, J., Fabião, F., Técnico, I. S., & Lisboa, U. T. De. (2009). Hydraulic Stability of Rubble Mound Breakwaters ' Armour Layer - Physical Model Study. Instituto Superior Técnico, Universidade Técnica de Lisboa, 1–11.
[43]. Rock Manual. (2007). Physical processes and design tools.
[44]. Shand, T. (2017). Guidance for coastal protection works. September 2018.
[45]. Smith E. S., and Abdel-Kader A. (1988). Coastal erosion along the Egyptian Delta. Journal of Coastal Research, 4(2), 245–255. http://www.jstor.org/stable/4297400%0Ahttp://about.jstor.org/terms
[46]. Ting, M. Z. Y., Wong, K. S., Rahman, M. E., & Meheron, S. J. (2021). Deterioration of marine concrete exposed to wetting-drying action. In Journal of Cleaner Production (Vol. 278, p. 123383). Elsevier Ltd. https://doi.org/10.1016/j. jclepro.2020.123383
[47]. Tulsi, Kishan, Schoonees, K., Ruthenavelu, M., Davids, G., Vonk, R., Stroh, F., & Herrington, N. (2016). Three-dimensional method for monitoring damage to dolos breakwaters. Proceedings of the Coastal Engineering Conference, 35 (December).
[48]. USACE. (2011). Coastal Engineering Manual-Part VI (USA (Ed.); Vol. 1100,). US Army Corps of Engineers. https://doi.org/10.1017/CBO9781107415324.004
[49]. Viet ND, Verhagen HJ, Vrijling JK, van Gelder PHAJM. (2008). Conceptual Design for the Breakwater System of the South of Doson Naval Base: Optimisation Versus Deterministic Design. Copedec Vii. 2008.
[50]. White K, El-Asmar HM, (1999), Monitoring changing position of coastlines using Thematic Mapper imagery, an example from the Nile Delta. Elsevier, Geomorphology 29 pp. 93–105.
[51]. imagery. International Journal of Remote Sensing, 27(14), 3025–3033. https://doi.org/10.1080/01431160600589179.
[52]. Zahra, Khyal A., (2018a). Adaptation to Climate Change Problems and Solutions on Magrour Idku and Idku Lake, Northwest Coast, Egypt. The 21st International Water Technology Conference (IWTC EGYPT), Ismailia, Egypt, 28:29, June 2018, pp. 69-92.
[53]. Zahra, Khyal A., (2018b), Assessment of implementation stages of submerged breakwater on the bay and shoreline at Al-Ahlam Sea Resort, Northwest Coast, Egypt, Ocean & Coastal Management, ScienceDirect, Elsevier, Volume 165, pp. 15-32.